NAVAL POSTGRADUATE SCHOOL
Monterey, California

THESIS

INTERNAL TIDAL BORES IN THE MONTEREY CANYON

by

Scott A. Key

December 1999

Thesis Advisor:	Leslie K. Rosenfeld
Second Reader:	Timothy P. Stanton

REPORT DOCUMENTATION PAGE

Public reporting burden for this collection of information is estimated to average 1 hour per response, including the time for reviewing instruction, searching existing data sources, gathering and maintaining the data needed, and completing and reviewing the collection of information. Send comments regarding this burden estimate or any other aspect of this collection of information, including suggestions for reducing this burden, to Washington headquarters Services, Directorate for Information Operations and Reports, 1215 Jefferson Davis Highway, Suite 1204, Arlington, VA 22202-4302, and to the Office of Management and Budget, Paperwork Reduction Project (0704-0188) Washington DC 20503.

1. AGENCY USE ONLY (Leave blank)	2. REPORT DATE December 1999	3. REPORT TYPE AND DATES COVERED Master's Thesis

4. TITLE AND SUBTITLE INTERNAL TIDAL BORES IN THE MONTEREY CANYON	5. FUNDING NUMBERS
6. AUTHOR(S) Key, Scott A.	

7. PERFORMING ORGANIZATION NAME(S) AND ADDRESS(ES) Naval Postgraduate School Monterey, CA 93943-5000	8. PERFORMING ORGANIZATION REPORT NUMBER

9. SPONSORING / MONITORING AGENCY NAME(S) AND ADDRESS(ES)	10. SPONSORING / MONITORING AGENCY REPORT NUMBER

11. SUPPLEMENTARY NOTES

The views expressed in this thesis are those of the author and do not reflect the official policy or position of the Department of Defense or the U.S. Government.

12a. DISTRIBUTION / AVAILABILITY STATEMENT Approved for public release; distribution unlimited.	12b. DISTRIBUTION CODE

13. ABSTRACT (maximum 200 words)

A thirty-four day record of near-bottom temperature and horizontal velocity spanning the lower third of the water column from within Monterey Canyon was examined. The observed internal tide is highly non-linear with kinetic energy dispersed among numerous overtides near the bottom and more concentrated in the primary semidiurnal constituent (M2) higher in the water column. The bottom currents and temperature vary in strength over the record period, taking on the characteristics of an internal bore at times with large up-canyon accelerations accompanied by rapid temperature drops. The bores are nearly phase locked to the sea level variations and arrive at the measurement site ~8.6 h after high tide in Monterey, CA. They are evident in the velocity records up to at least 35 m above the bottom and may be accompanied by high frequency pulses that extend higher. The variation is not caused by direct forcing from the barotropic tidal range as the strongest bores do not exclusively occur during either the spring or neap phase of the barotropic tide. Speculation on the cause for the temporal variation centers on the changes in mid-water stratification observed.

14. SUBJECT TERMS internal wave, internal bore, tidal bore, internal tides, tides, waves	15. NUMBER OF PAGES 104
	16. PRICE CODE

17. SECURITY CLASSIFICATION OF REPORT Unclassified	18. SECURITY CLASSIFICATION OF THIS PAGE Unclassified	19. SECURITY CLASSIFI- CATION OF ABSTRACT Unclassified	20. LIMITATION OF ABSTRACT UL

THIS PAGE INTENTIONALLY LEFT BLANK

INTERNAL TIDAL BORES IN THE MONTEREY CANYON

Scott A. Key
Lieutenant, United States Navy
B.S., University of Washington, 1993

Submitted in partial fulfillment of the
requirements for the degree of

MASTER OF SCIENCE IN PHYSICAL OCEANOGRAPHY

from the

NAVAL POSTGRADUATE SCHOOL
December 1999

THIS PAGE INTENTIONALLY LEFT BLANK

ABSTRACT

A thirty-four day record of near-bottom temperature and horizontal velocity spanning the lower third of the water column from within Monterey Canyon was examined. The observed internal tide is highly non-linear with kinetic energy dispersed among numerous overtides near the bottom and more concentrated in the primary semi-diurnal constituent (M2) higher in the water column. The bottom currents and temperature vary in strength over the record period, taking on the characteristics of an internal bore at times with large up-canyon accelerations accompanied by rapid temperature drops. The bores are nearly phase locked to the sea level variations and arrive at the measurement site ~8.6 h after high tide in Monterey, CA. They are evident in the velocity records up to at least 35-m above the bottom and may be accompanied by high frequency pulses that extend higher. The variation is not caused by direct forcing from the barotropic tidal range as the strongest bores do not exclusively occur during either the spring or neap phase of the barotropic tide. Speculation on the cause for the temporal variation centers on changes in mid-water stratification observed.

THIS PAGE INTENTIONALLY LEFT BLANK

TABLE OF CONTENTS

THIS PAGE INTENTIONALLY LEFT BLANK

LIST OF FIGURES

ACKNOWLEDGEMENT

THIS PAGE INTENTIONALLY LEFT BLANK

I.   INTRODUCTION

A.   MOTIVATION

1.   Background

Internal waves are prevalent throughout the world's oceans. An internal wave is a gravity wave within a fluid of variable density. Almost any measurement taken in the ocean will contain signals of internal waves (Munk 1981). Internal waves can even have a surface signature of alternating bands of smooth and rough seas given the correct conditions (Munk 1981). Numerous studies have been conducted to try and link internal waves to other ocean processes.

Internal waves are thought to play a major role in the distribution of energy in the ocean (Munk 1997). An empirical energy spectrum (GM79) of internal waves was proposed in 1979 (Garrett and Munk 1979) for the open ocean. This spectrum has been used as a benchmark for comparison with measurements taken in the various parts of the ocean. Internal wave energy has been found to exceed the GM79 spectrum in coastal regions. Huthnance (1989) speculated that the GM79 spectrum is valid with some localized deviations near and on the continental shelf. Eriksen (1998) has recorded increased energy levels compared to GM79

at frequencies that correspond to the local critical frequency for sloping terrain.

Internal waves in submarine canyons exert effects on the sediment transport, biology, and even on the water properties of the continental shelf farther up-canyon. Submarine canyons act like funnels moving water onto the continental shelf (Huthnance 1989, Lafuente 1999). Most internal waves will be "trapped" and funneled farther up-canyon by the walls that are supercritical for all but the shortest period internal waves, while the floor is generally subcritical (summarized in Petruncio *et al.* 1998). When the canyon's bottom slope happens to be near the critical slope for one of the major tidal constituents, bottom intensification of the tidal currents, or even an internal tidal bore, may be found (Thorpe 1992, Ostrovsky and Stepanyants 1989). Petruncio *et al.* (1998) found the Monterey Canyon's bottom slope to be near critical for the M2 tidal frequency, causing intensified bottom tidal currents. Shea and Broenkow (1982) observed large magnitude internal tides in the canyon and what may have been an internal tidal bore near the canyon head. Cacchione (1999) has pointed out that the slope of many submarine canyons is close to being critical for the M2 tide. As such, the Monterey Canyon may be representative in its effects on the internal wave field.

2. Experiment Setup

Submarine canyons are an under-sampled region compared to more 2-dimensional areas of the continental shelf. The steep topography makes it very difficult to obtain oceanographic measurements via moorings or cable-lowered instruments. Little is known about internal wave spatial scales in canyons where interaction with the steep topography is likely to facilitate more rapid transfer of energy toward smaller scales and turbulence production. Because of their lateral and vertical heterogeneity, canyons are difficult to characterize with a few point observations. One way to overcome this problem is to conduct profile surveys that would provide a broad spatial coverage. A National Science Foundation (NSF) funded experiment was conducted in the Monterey Canyon by Leslie Rosenfeld (Naval Postgraduate School) and Eric Kunze (Univ. of Washington) with the following objectives taken from the grant proposal for the experiment.

- Determine the finescale shape and level of the vertical wavenumber spectra for vertical displacement and horizontal velocity as compared with the open ocean GM79 model.
- Determine the spatial scales and heterogeneity of the internal wave field as a function of vertical, along and cross-canyon position. A specific issue

of interest is how much energy negotiates the sharp bends in the canyon versus being back reflected.

- Determine the anisotropy of the internal wave field to evaluate where the dominant semidiurnal tide is best described as propagating and where as standing.

- Intercompare dissipation rates inferred from the up-canyon energy-flux divergence, and the finescale shear and strain spectra using the Gregg-Henyey-Polzin scaling.

The experiment collected numerous measurements taken both by moored and shipboard instruments. For canyon depths between 500 and 1600 m, full-water-depth velocity, density and dissipation profiles were made using Sippican velocity and CTD profilers and Lueck's expendable dissipation profilers (which failed to return useful data). In canyon depths shallower than 300 m, over the canyon rim and on the adjacent shelf region, fine- and microstructure measurements were collected by Michael Gregg (Univ. of Washington) in a closely associated experiment. In an effort to bridge the deep and shallow experimental domains, moorings with upward facing acoustic Doppler current profilers (ADCP's) were placed between 300-m and 400-m depth to give a month-long time series of the lower water column currents. Two 12-h time series of CTD casts were made over the canyon near 400-m depth, and two near 800-m depth. This thesis will

4

concentrate on the data collected by CTD's and moored instruments.

B.   INTERNAL WAVE THEORY

1.   Linear Internal Wave Theory

Linear wave theory is a very well understood and widely applicable wave theory. Internal gravity waves are described by linear theory as easily as surface gravity waves. Internal waves can be formed at the boundary between two fluids of different densities or in a continuously stratified fluid.

a)   *Dispersion Relation*

The dispersion relation defines how a wave type behaves. More specifically, the dispersion relation relates the angular frequency and the wave number of any given wave. This relation is different for every type of wave and the dispersion relation for internal gravity waves reveals unique characteristics about them.

Starting with the basic conservation equations from Kundu (1990) and including the Boussinesq approximation with the inviscid fluid approximation yields:

$$\frac{\partial u}{\partial t} - fv = -\frac{1}{\rho_0}\frac{\partial p}{\partial x} \tag{1}$$

$$\frac{\partial v}{\partial t} + fu = -\frac{1}{\rho_0}\frac{\partial p}{\partial y} \tag{2}$$

$$\frac{\partial w}{\partial t} = -\frac{1}{\rho_0}\frac{\partial p}{\partial z} - \frac{\rho g}{\rho_0} \tag{3}$$

$$\frac{\partial u}{\partial x} + \frac{\partial v}{\partial y} + \frac{\partial w}{\partial z} = 0 \tag{4}$$

$$\frac{D\rho}{Dt} = 0 \tag{5}$$

Equations (1) through (5) contain five unknowns: horizontal velocity (u, v), vertical velocity (w), density (ρ), and pressure (p). Equation (5) is a result of the assumption that water is an incompressible fluid.

Assuming that the system is starting at a steady state of no motion, a hydrostatic balance will exist and the vertical acceleration will be initially zero.

$$\frac{\partial w}{\partial t} = 0 = -\frac{1}{\rho_0}\frac{\partial p}{\partial z} - \frac{\rho g}{\rho_0} \tag{6}$$

In order to for waves to appear, motion must develop that will disturb the initial pressure and density fields. We can describe the motion effects on density and pressure in terms of a mean quantity and a fluctuating quantity.

$$p = \bar{p}(z) + p'(x, y, z, t) \tag{7}$$

$$\rho = \bar{\rho}(z) + \rho'(x, y, z, t) \tag{8}$$

Now we must use equations (7) and (8) to describe a water particle's motion due to the now present wave

action. This is done by substituting equations (7) and (8) into the equations of motion (1-5). Because we assumed that there was some previously existing steady state that is now being perturbed, the gradients of the mean quantities will be dropped since they only describe the state of no motion. Since we are dealing with linear wave theory, all of the non-linear terms are also neglected.

$$\frac{\partial u}{\partial t} - fv = -\frac{1}{\rho_0}\frac{\partial p'}{\partial x} \tag{9}$$

$$\frac{\partial v}{\partial t} + fu = -\frac{1}{\rho_0}\frac{\partial p'}{\partial y} \tag{10}$$

$$\frac{\partial w}{\partial t} = -\frac{1}{\rho_0}\frac{\partial p'}{\partial z} - \frac{\rho'g}{\rho_0} \tag{11}$$

$$\frac{\partial u}{\partial x} + \frac{\partial v}{\partial y} + \frac{\partial w}{\partial z} = 0 \tag{12}$$

$$\frac{\partial \rho'}{\partial t} - \frac{N^2\rho_0}{g}w = 0 \tag{13}$$

where $N^2 \equiv -\frac{g}{\rho_0}\frac{\partial \overline{\rho}}{\partial z}$ is known as the Brunt-Väisälä frequency or buoyancy frequency. This is the frequency at which a fluid particle will oscillate if it is vertically disturbed from its equilibrium location.

The task now is to use the new equations of motion to derive an equation that describes the vertical motions of the water particles in time and space. This is done by combining the time derivative of the continuity equation

7

(12) and the directional derivatives of the horizontal momentum equations (9,10).

$$\frac{1}{\rho_0}\nabla_H^2 p' + f\left(\frac{\partial u}{\partial y} - \frac{\partial v}{\partial x}\right) = \frac{\partial^2 w}{\partial z \partial t} \qquad (14)$$

where $\nabla_H^2 \equiv \partial^2/\partial x^2 + \partial^2/\partial y^2$ is known as the horizontal Laplacian operator.

Equation (14) is still an equation of multiple variables. The elimination of pressure from the equation can be accomplished by first taking the time derivative of equation (11) and using equation (13).

$$\frac{1}{\rho_0}\frac{\partial p'}{\partial z \partial t} = -\frac{\partial^2 w}{\partial t^2} - N^2 w \qquad (15)$$

Now the horizontal Laplacian of equation (15) is taken and substituted into the time and depth derivative of equation (14).

$$\frac{\partial^2}{\partial z \partial t}\left(\frac{\partial^2 w}{\partial z \partial t}\right) - f\frac{\partial^2}{\partial z \partial t}\left(\frac{\partial u}{\partial y} - \frac{\partial v}{\partial x}\right) = \nabla_H^2\left(\frac{\partial^2 w}{\partial t^2} - N^2 w\right) \qquad (16)$$

Rewriting equation (16) with the assumption that N^2 is horizontally independent and using the directional derivatives of equations (9,10) and the continuity equation (12) yields a differential equation for the vertical motion.

$$\frac{\partial^2}{\partial t^2}\nabla^2 w + N^2\nabla_H^2 w + f^2\frac{\partial^2 w}{\partial z^2} = 0 \qquad (17)$$

where ∇^2 is the three dimensional Laplacian operator.

Equation (17) is a second order, homogeneous, and separable differential equation. An assumed solution to this equation is a periodic wave.

$$w = w_0(z)e^{i(kx+ly-\omega t)} \tag{18}$$

If the assumed solution is substituted into the differential equation and the terms arranged, we get the governing equation for internal waves from which the dispersion relation is easily shown.

$$(-i\omega)^2 \left[(ik)^2 + (il)^2 + \frac{d^2}{dz^2} \right] w_0 + N^2 \left[(ik)^2 + (il)^2 \right] w_0 + f^2 \frac{\partial^2 w_0}{\partial z^2} = 0 \tag{19}$$

$$\Rightarrow \frac{\partial^2 w_0}{\partial z^2} + \frac{(N^2 - \omega^2)(k^2 + l^2)}{\omega^2 - f^2} w_0 = 0 \tag{20}$$

Assuming the vertical structure is of the form e^{imz}, the dispersion relation is defined as

$$m^2 \equiv \frac{(N^2 - \omega^2)(k^2 + l^2)}{\omega^2 - f^2} \tag{21}$$

The dispersion relation gives equation (20) two types of solutions. The first type is an exponential solution and occurs when $(\omega > N)$ or $(\omega < f)$. In order for the equation (20) to have a wave solution, the frequency must be bounded by $f < \omega < N$. This is the necessary condition for freely propagating internal gravity waves to exist.

b)   *Internal Wave Reflection*

Internal waves are difficult to visualize for most people.   To help in their visualization, Munk (1981) suggests looking at a wave packet with crests and troughs along planes normal to the page and inclined with respect to the (x,z) axis as shown in Figure 1.   The phase velocity is in the direction of $\bar{k}$ (wave number vector) normal to the crests, and the group velocity C_g is parallel to the crests. The net result is that the wave packet appears to slide sideways.   The angle of the wave number vector ($\bar{k}$) relative to the horizontal can be found from:

$$\tan\theta = \frac{m}{k_H} = \left(\frac{N^2 - \omega^2}{\omega^2 - f^2}\right)^{1/2} \tag{22}$$

This results in a steep angle of phase propagation when the internal wave frequency is near the inertial frequency $(\omega \approx f)$; and in a flat angle of phase propagation when the internal wave frequency is near the buoyancy frequency $(\omega \approx N)$.   The group velocity is directed 90° from the phase velocity with vertical component of opposite sign. This means that for near-inertial frequencies, $(\omega \approx f)$, the packet of energy will propagate at near horizontal; and at near-buoyancy frequencies $(\omega \approx N)$, the energy packet will propagate at near vertical.   In both cases, linear theory holds that the group velocity will approach zero as the

internal wave frequency approaches either the $\omega \approx f$ or the $\omega \approx N$ limit.

When internal waves reflect, the angle of incidence relative to the horizontal equals the angle of reflection relative to the horizontal. This is an important distinction from other types of waves that preserve their angle relative to the reflecting surface. Figure 2 illustrates the geometry of internal wave reflection. In the figure, z' is the vector normal to the reflecting surface, α is the slope of the reflecting surface, x' is the vector parallel to the reflecting surface, g is the gravity vector, and θ is the angle with respect to the horizontal at which the internal wave group propagates.

Because of the horizontal angle reference, internal waves have three types of reflection: subcritical, supercritical, and critical. Subcritical reflection occurs when the slope of the reflecting surface is less than the angle of energy propagation for the wave packet (referenced to the horizontal). These waves will be forward reflected towards shallower waters. Supercritical reflection occurs when the reflecting surface has a slope steeper than the angle of wave energy propagation. These waves will be back reflected towards deeper water, where they will likely dissipate in the open ocean (Munk 1981). Critical reflection occurs when the slope of the reflecting surface

is equal or nearly equal to the angle of wave energy propagation. At critical reflection angles, linear wave theory develops a singularity (Huthnance 1989). Energy density becomes infinite and group velocity falls to zero, violating the underlying linear assumptions. The result of this may be the formation of non-linear effects such as a bore or other hydraulic jump traveling up the slope of the reflecting surface (Slinn and Riley 1996).

2. Non-Linear Internal Wave Theory

Internal waves are not fully described by linear wave theory. Numerous observations have shown that many of the features of internal waves can only be explained by non-linear theories (Garrett and Munk 1979). Non-linear wave theory is a complicated subject, so only a very small portion of it will be discussed here. For a more complete summary of non-linear internal wave theories, see Ostrovsky and Stepanyants (1989).

A soliton is a solitary non-linear wave. A soliton can exist either as a surface gravity wave or as an internal wave. They have been observed in both forms in nearly every part of the world's oceans (Ostrovsky and Stepanyants 1989). A balance between the non-linear steepening of the wave and dispersive effects results in the form of a soliton being a single hump propagating at a phase speed that increases with the amplitude of the soliton. Various non-linear theories can adequately describe the soliton. These include, but are

not limited to, the KdV, modified KdV, Joseph, and Smooth Stratification Model. Perhaps the most often used theory to describe the non-linear internal waves is the Korteweg-de Vries (KdV) solution. A soliton is one of two possible solutions to the Korteweg-de Vries equation, the other being a train of cnoidal waves. However, caution must be used when applying these theories to solitons or bores as most non-linear theories assume that the non-linearity will be weak (Ostrovsky and Stepanyants 1989). The ratio of nonlinear to dispersive effects $\left(a\lambda^2/H^3\right)$ is used to determine how the form of a soliton will change over time where a is the amplitude of the solitary wave, H is the depth of water the wave is in, and λ is the wavelength of the solitary wave. When the ratio has a value of less than 16, the non-linear effects can balance the dispersive effects and the soliton maintains a constant form, however when the ratio is greater than 16 the non-linear effects overpower the dispersive effects and lead to a steeping wave front eventually causing a hydraulic jump (Kundu 1990). Perhaps the simplest model of a hydraulic jump is the 2-layer hydraulic jump model used by Holloway (1987). Figure 3 shows a diagram of this model. In the figure, h_2' is the initial bottom layer thickness with velocity u_2', and h_2 is

13

the bottom layer height after the hydraulic jump with velocity u_2.

Holloway (1987) defines the conditions required for a hydraulic jump in terms of the Froude number (F)

$$F^2 = \frac{u_1^2}{g'h_1} \tag{23}$$

where $g' = (\rho_2 - \rho_1)g/\rho_2$.

He defines a critical F where it becomes possible for a jump to occur as:

$$F_c = \left[\frac{1 + \dfrac{h_1}{H}\left(\dfrac{u_2^2}{u_1^2}\right)^2}{1 - \dfrac{h_1}{H}} \right]^{\frac{1}{2}} \tag{24}$$

with h_1, H, u_1, u_2 from Figure 3, which shows a downward jump in the upper layer if the front is considered stationary. For a moving jump, flows relative to the jump speed should be used in equations (23) and (24). He found that hydraulic jumps occurred approximately three hours after F became critical at a value of F much larger than F_c, generating a larger hydraulic jump than would have been possible if F had just barely been super-critical (Holloway 1987). The largest downward jumps were found to exist when there was a thin upper layer present over a weak lower layer flow.

Surface jumps are common throughout the world, from spillways on dams to jumps near large rocks in quickly

flowing rivers. A bore is a propagating hydraulic jump. These are less common than stationary jumps. Surface bores have been observed in a few rivers and inlets while internal bores have only rarely been observed (Halpern 1971, Holloway 1987). Tidal bores in rivers are formed by interactions between the tidal wave and the narrowing river channel. Basically the tidal wave will grow as the tidal energy is confined to a smaller and smaller area until it becomes unstable and develops into a hydraulic jump (tidal bore). These tidal bores tend to be largest during the spring tides (Pugh 1987). The tidal bore on the Severn in England is an excellent example of a surface bore.

C. OBSERVATIONS OF NON-LINEAR INTERNAL WAVES ON CONTINENTAL SHELVES AND SEAMOUNTS

Lee and Beardsley (1974) used data collected from Massachusetts Bay by Halpern (1971) to compare with a non-linear KdV-type wave in an effort to determine the relative importance of non-linearity and dispersion on the generation of large amplitude internal waves in the breakdown of internal fronts. They found that their model adequately described the physical features found by Halpern in his observations of tidally generated internal waves.

Howell and Brown (1985) found soliton packets on the Northern California continental shelf during the Coastal Ocean Dynamics Experiment in 1981. They concluded that the internal solitary waves are generated on the continental

15

shelf and evolve into soliton packets as they propagate shoreward.

Holloway *et al.* (1997) use a numerical solution to the KdV equations to model the evolution of an initially sinusoidal long internal wave to represent an internal tide. Their model shows a transformation of the initial waveform into a series of shocks and solitons as it propagates over the continental shelf. Their model was run using hydrographic data from observations made over the Australian Northwest Shelf.

Stanton and Ostrovsky (1998) reported strong solitons off the Oregon coast. Extremely strong solitary internal wave packets were observed over a three-week period on a very shallow and strongly stratified pycnocline off northern Oregon. During periods of the strongest tidal forcing, solitons were consistently observed on the leading edge of a semidiurnal tidal bore, with pycnocline displacements of up to 25 m downward from a 7-m initial depth. The extreme non-linearity of these observations are beyond the limits of the weak non-linearity assumed by the KdV model. A higher order model, the "CombKdV model", is proposed to describe the observations. The higher order model, despite its assumption of still weak non-linearity, closely matches the observed data.

Eriksen (1998) observed internal wave structures as they reflected off the Fieberling Guyot seamount in the

North Pacific Ocean. His observations were quite long, lasting approximately one year. He observed that the records substantially differed from the predictions of linear wave theory. Some interesting observations were the size of the reflections and the presence of a critical slope reflection. The effects of internal wave reflections in the primary mode of the EOF's were detectable at 750 m above the seafloor. These reflections had a phase structure that conformed to the linear theory predictions, but the amplitude decayed in proportion with the EOF wave number. Intensifications of the wave spectrum with respect to the GM79 spectrum were seen at the local critical frequency. The near bottom water was well mixed due to large and frequent density overturnings caused by the wave reflections.

D. INTERNAL WAVE WORK IN MONTEREY AND OTHER CANYONS

The Monterey Canyon is located nearly in the middle of Monterey Bay, California. Its upper reaches approach the coast to within a few hundred meters at Moss Landing, California, making it very attractive for deep-sea experiments and observations. Both Moss Landing Marine Laboratories and the Monterey Bay Aquarium Research Institute (MBARI) are located near the canyon head and make frequent, mainly biological and geological, measurements in the canyon. The surface tide in Monterey Bay is of the

17

mixed semi-diurnal type and essentially co-oscillates (Petruncio *et al.* 1998), with a strong internal tide in the Monterey Canyon (Petruncio *et al.* 1998).

Broenkow and McKain (1972) observed tidal oscillations over a 25-h period from two locations 3 km apart. Their measurements revealed semidiurnal isopycnal oscillations with maximum ranges of 80 m propagating shoreward at 20 to 30 cm/s.

Shepard *et al.* (1979) found current oscillations with periods of eight to nine hours that were dominated by the overtides rather than the semi-diurnal internal tide from three 4-day records of current measurements recorded at 3 m and 30 m over the canyon floor. They demonstrate some of the difficulties with observations in Monterey Canyon. Unlike many of the other canyons discussed by them, the Monterey Canyon does not generally have water flow that is aligned with the canyon axis. They speculated that there may be many more tributary canyons or that the canyon topography is just much more complicated than believed at the time. As the hydrographic survey conducted by MBARI in 1998 showed, their thoughts on the canyon topography were correct; Monterey Canyon has a very complicated structure.

Shea and Broenkow (1982) used data collected by Broenkow and McKain (1972) and data collected in 1978 and 1979 to further analyze the internal tidal signal looking for evidence of nutrient enrichment. They found an internal

18

tide with heights ranging from 50 to 120 m and the presence of a breaking internal bore 25 m above the bottom near the canyon head. The bore was identified using a thermistor just offshore of the Moss Landing harbor entrance.

The Monterey Bay National Marine Sanctuary site characterization, physical oceanography section (Broenkow) reports internal tidal displacements with magnitudes of up to 120 m just 5 km from the canyon head. Other measurements are cited from Heard (1992) with 60 m internal tidal amplitudes in 185 m of water near the canyon head.

Petruncio *et al.* (1998) analyzed data from ITEX1 and ITEX2 experiments conducted in Monterey Bay during April and October, 1994, respectively. Vertical profiles of temperature, salinity, and velocity (excluding the bottom 20 to 30% of the water column) were made at one to two hour intervals over 25-h periods during each experiment. They found semidiurnal currents in the 20 cm/s range, an order of magnitude larger than the estimated barotropic tidal currents. They proposed a link between surface and internal tides as they relate to the stratification of the water. Shoreward energy propagation was observed during ITEX1 and a standing wave (internal seiche) during ITEX2. They speculate that this was due to differences in the stratification present in Monterey Bay during April and October when the two experiments were carried out.

19

Their analysis of the internal tide was limited by design of the experiments to describing the linear internal tide. Based on the assumption that the linear internal tide can not negotiate the sharp bends in the canyon, two possible generation sites, Smooth Ridge and Steep Ridge, for the locally observed internal tidal signal were identified.

Lafuente (1999) examined the La Linea Canyon in the western Alboran Sea. He focused his measurements on the shallower areas of the canyon (< 100 m), but did make some measurements in the deeper areas (~300 m). He found that the deeper tidal currents exhibited large amplitudes (~50 cm/s) and were phase locked with the more barotropic tidal currents near the surface.

Matsuyama *et al.* (1993) measured the near-bottom currents in the Suruga Trough in Japan. They found the currents were dominated by the M2 semi-diurnal tidal constituent, which was five times the strength of the next strongest constituent. The near-bottom currents seemed to be phase locked near 0° with the sea level while the barotropic tidal currents were 90° out of phase with the sea level.

Takeuchi and Hibiya (1997) made observations near the Suruga Trough in Uchiura Bay. They identified a generation site for the internal tide in Uchiura Bay and conducted measurements in the area. They discovered that the

character of the internal tide in the bay was dependent on the non-linear dynamics at the generation site.

THIS PAGE INTENTIONALLY LEFT BLANK

II. DATA COLLECTION

A. MOORED

Data were collected in the Monterey Canyon over a 34-day period from 05 August 1997 until 10 September 1997. Two moorings, BB and NB, were deployed approximately 2.8 km apart from each other after a brief bathymetric survey was conducted (Figure 4). The moorings were lowered to within 10 m of the bottom before being released. Both were intended to be close to the middle of the canyon axis, but high resolution bathymetry obtained the following summer by MBARI revealed that BB was on the axis at the apex of a curve in the canyon, while NB was off the principal axis on the southern flank of the canyon (Figure 5). MBARI obtained their high-resolution bottom topography using a Simrad 300 bottom mapping system. It has a vertical resolution of 0.1% of the water depth and a horizontal resolution of 2% of the water depth.

Both moorings were short, taut moorings consisting of a railroad wheel anchor, two acoustic releases and an upward looking, self-contained ADCP deployed in a foam buoy. An Alpha Omega thermistor was attached to the metal frame protruding from below the buoy.

One mooring, NB, supported a RD Instruments 300 kHz narrowband ADCP in a 48" diameter buoy. The ADCP transducer

23

was 6 m above the seafloor in ~390 m of water and resolved currents in 4-m bins with the deepest bin centered 12 m above the bottom. Velocity data were calculated by vector averaging the results from 270 pings spaced evenly over 3-min intervals. RDI reports a nominal standard deviation due to instrument error of 0.8 cm/s for a 270-ping average for the narrowband ADCP. The Alpha Omega temperature recorders employ a YSI 46006 thermistor with ±0.03 °C stability. The instruments were calibrated by the Oregon State University mooring group immediately prior to the experiment. The clocks maintained accuracy to within 40 s over the course of the experiment. The thermistor was located 6 m above the bottom and recorded instantaneous temperatures at 1-min intervals.

The second mooring, BB, supported a RD Instruments 300 kHz broadband Workhorse ADCP in a 37" foam sphere. The ADCP was 6 m above the bottom in ~333 to 337 m of water. The depth of the BB mooring was determined by comparing the pressure sensor in the ADCP, the fathometer readings taken from the R/V *Pt. Sur* during deployment, and DGPS- determined location relative to the high-resolution bathymetry data collected by MBARI in the spring of 1998. For the purposes of this analysis, the depth of the BB mooring anchor will be taken as 333 m. It resolved currents in 4-m bins with the deepest bin centered 12 m above the bottom. Velocity data

were determined by vector averages of 12 pings spaced evenly over 1.5 min intervals. RDI reports a nominal standard deviation due to instrument error of 0.8 cm/s for a 12-ping average for the Workhorse ADCP. The BB thermistor recorded an instantaneous temperature at 6 m above the bottom at 1-min intervals. Both ADCP's recorded velocity data in earth coordinates and an instantaneous value of pitch and roll in each ensemble header at 1.5-min(BB) or 3 min(NB) intervals.

The BB and NB moorings were placed in such close proximity, and used similar sampling schemes, to provide redundancy in case of failure of one of the moorings. As will be seen, both instruments worked well and the records show a high degree of spatial variability in the canyon.

ADCP's use backscattered sound to measure velocity. The Doppler effect is used by transmitting sound at fixed frequencies and listening to the returning echoes from sound scatterers in the water. The sound is scattered from the small plankton and particles in the water column, which are assumed to have, on average, the same horizontal velocity as the water that they are in. The frequency reflected by the sound scatterer is shifted lower when the scatterer is moving away from the ADCP and shifted higher when the scatterer is moving towards the ADCP. As the Doppler shift is only sensitive to along-beam motion, the components of flow along several radial directions, and the orientation of

the transducers, must be measured to estimate the full velocity vector.

The ADCP's used in this experiment have four acoustic beams which can determine three orthogonal components of velocity, with redundancy. The four transducers are arranged in a Janus configuration that allows beams on opposite sides of the square to act as a pair. The method assumes the velocity field is horizontally homogeneous over the area ensonified by the four transducers. Due to the large influence of mooring motion on vertical velocity estimates, only horizontal components of velocity were resolved in these data.

We considered that the mooring motion may have introduced possible errors in the horizontal velocity data as well. While the maximum pitch and roll recorded by the tilt sensors records on the two ADCP's was 3.5°, well within the ± 15° operating range specified by RDI, the maximum angular acceleration was 2.3° per min for the BB ADCP. Knowing that the large angular accelerations experienced by surface moorings can contaminate ADCP velocity measurements, several messages were exchanged with RDI on the response of the tilt correction algorithms to rapid (on the order of minutes) tilt angle changes. At this time we do not have full characterization of the reaction time of the tilt correction.

Velocity data degraded by erroneous tilt values are typically seen as rapid accelerations/decelerations that are coherent throughout the measured water column. Even though no coherent changes were present in the records during the strong tilting events, two further steps were taken to convince us of the validity of the measured velocities. To get an order of magnitude estimate for the possible errors in the data due to any uncorrected tilt angles, calculations were performed on a typical tilt excursion. Using a maximum tilt angle of 3° in a 1.5-min interval, the maximum speed deviation found to exist is less than 7 cm/s. An analysis of the mooring motion confirmed that the measured tilts were consistent with the predicted instrument deflections based on the recorded currents.

B.   SHIPBOARD

Four 12-h CTD time series were taken from the R/V Pt Sur. The length of each series was limited by the need to turn the ship over to the operators of the opposing 12-h watch. CTD stations are marked on Figure 4 as square boxes, the station between the two moorings is known as "Shallow" and the other station is known as "Deep". Measurements were taken at Shallow on 09 and 21 August 1997 and at Deep on 10 and 20 August 1997 using a 9/11 SeaBird CTD along with a SeaTech light transmissometer with a 25 cm path length. CTD casts were conducted at Shallow approximately every 30-min

from 0708Z - 1848Z 09 August 1997 and again from 1029Z - 2140Z 21 August 1997.

Current data were recorded by a 150-kHz ADCP (VM-ADCP) mounted in the hull of the R/V *Pt Sur* while CTD casts were being conducted. The VM-ADCP calculated average currents over either a 3-min or a 1-min interval. The ship's heading and velocity, obtained from gyrocompass and differential GPS inputs respectively, are needed to obtain earth-referenced water velocities. Some of the VM-ADCP data was found to be unusable due to problems with either the GPS and/or gyrocompass interface and were not used in this analysis.

C.   TIDE GAUGE

Sea level data were obtained from tide gauge No. 941-3450, located in Monterey, California and maintained by NOAA. The gauge can be found in the harbor maintenance supervisor's office at the seaward end of Municipal Wharf No. 2 in Monterey.

The sea level data are collected using the Next Generation Water Level Measurement System which uses an acoustic measurement device rather than the older float type system. The water level is measured by sending a shock wave of acoustic energy down a half-inch diameter pipe and measuring the travel time using a calibrated reference. Another change from older stilling well float measurements is in the well itself. The new protective well is more

28

exposed than the stilling wells were, allowing more of the wind waves and chop to affect the sea level measurements. Acoustic measurements are recorded every 6 min from the average of a set of 181 1-s interval measurements. Data recorded are the mean sea level, standard deviation, and the number of outliers with a resolution of 0.01 feet. Hourly data, obtained from NOAA's web site, were used in all the figures presented here, with the exception of Figure 17 and Figure 18 which used the times of high and low sea level to the nearest 6 min.

D.   ANCILLARY

Various other data have been used to corroborate assorted findings. These include: AVHRR data from NOAA satellites, data from various buoys in Monterey Bay placed by MBARI, and surface currents derived from a CODAR type HF radar system operational in Monterey Bay.

THIS PAGE INTENTIONALLY LEFT BLANK

III. ANALYSIS AND RESULTS FOR FULL TIME SERIES

A. PRINCIPAL AXES

Data from the two ADCP's was recorded in earth referenced coordinates, but the currents from the two moorings do not lie along either the North/South or the East/West axis. To further complicate data analysis, the up- and down-canyon currents are not aligned 180° apart from each other.

Two methods were used to find the "best" way to calculate the principal axes for the current data. The first method calculates the principal axes by assuming the up-canyon direction is in the NE quadrant and the down-canyon direction is somewhere in the other three quadrants. Once the principal axes are calculated the current data are projected onto the derived axes (Figure 6). Data in the NE and SW quadrants are projected onto the positive and negative A' axis respectively, while data in the NW and SE quadrants are projected onto the negative and positive A" axis respectively. The second method created two least-squares-fit lines from current data in the u>0 and u<0 regions separately. The results of the two principal axes calculations are show overlain on the current data from BB bin #1 (Figure 7) and a comparison between the original speeds and the speeds along the new along-canyon axes was

31

completed (Figure 8). Negative values indicate westward flow in the original data and down-canyon flow in the rotated data. It is clear that the first method is superior to the second, replicating virtually all of the variance in speed seen in the original data.

Figure 9 and Figure 10 show velocity scatter plots for four depth bins at NB and BB respectively with the derived principal axes from method one shown. The calculated near-bottom along-canyon axes at both mooring locations are in general agreement with the expected directions given the topography at the mooring sites (Figure 5). The principal axes directions at the BB location show more variability with depth than at the NB location; this is attributed to the location of the BB mooring near a sharp bend in the canyon topography. The component of flow along the principal axis in the NE quadrant is subsequently referred to as "up-canyon", while the component of flow along the principal axis in the NW or SW quadrant, depending on bin number, is referred to as "down-canyon".

B.   POWER SPECTRA

Spectral analysis was performed on the current records obtained from the BB ADCP. The spectra were calculated by averaging the fast Fourier transform results from 9600-point Hamming windowed pieces (corresponding to a 240 h time period) overlapped by 50%. In addition to the piece

averaging, each bin's spectrum has been frequency averaged from 0.3-cph onward with a linearly increasing average length. As expected, there was a strong spectral peak at the M2 frequency (12.42 h) (Petruncio *et al.* 1998). Figure 11 shows the kinetic energy spectra for all 29 depth bins from the mooring, with each bin separated on the y-axis by one decade. In addition to the prominent semidiurnal peaks, numerous overtides are clearly seen, including peaks at the M3, M4, 2MK5, M6, and 3MK7 frequencies. We have examined the spectra all the way out to the Nyquist frequency and there are no discernable humps or change in slope near the Brunt-Väisälä frequency.

The kinetic energy spectra for the top (bin #29) and bottom (bin #1) depth bins, 124 and 12 m above the bottom, respectively, were compared to the kinetic energy spectra for open ocean internal waves developed by Garrett and Munk (GM79) (Figure 12). The kinetic energy for both depths is higher than predicted by GM79 and the near-bottom kinetic energy is higher than the shallower kinetic energy. The near-bottom spectrum's peaks at the M3, 2MK5, and M6 frequencies are nearly the same level as the peak at the M4 frequency for the shallower spectra.

C.   TIDAL ANALYSIS

Tidal analysis, resolving 35 different tidal constituents, was performed on the current records. It was

found that the kinetic energy of the deeper currents was spread out more evenly over the various constituents than the shallower currents.

Table 1 summarizes the differences between the depth bins for selected tidal constituents. The strength of the odd numbered shallow-water constituents in many bays and narrow estuaries are typically not very strong in semi-diurnal tidal regimes, however mixed tidal regimes may have the fifth-diurnal tides enhanced (Pugh 1987). In the canyon, which may be thought of as like a river, the fifth-diurnal tide is enhanced, stronger than the M6 at some depths. The third and seventh-diurnal tides are also enhanced in our data. Curiously the third-diurnal tide has a minimum in the middle depth bins while the other odd numbered constituents have a maximum in the middle depth bins.

Table 1   Maximum Current Speed (cm/s) for Selected Tidal Constituents

Constituent		at BB mooring									
Name	cph	321 m	309 m	297 m	285 m	273 m	261 m	249 m	233 m	221 m	213 m
K1	.0418	3.37	3.85	3.89	3.70	3.49	3.41	3.38	3.04	2.40	1.88
M2	.0805	8.24	8.64	8.38	8.00	7.86	7.97	8.28	8.95	9.96	11.39
M3	.1208	1.00	0.82	0.67	0.78	0.90	1.17	1.34	1.31	1.25	1.17
M4	.1610	4.12	3.86	3.10	2.26	1.64	1.93	2.10	2.10	1.98	2.16
2MK5	.2028	0.78	1.12	1.18	1.13	1.02	0.91	0.93	0.83	0.84	0.70
M6	.2415	1.14	1.04	1.04	0.87	0.59	0.54	0.75	0.80	0.80	0.64
3MK7	.2833	0.44	0.70	0.58	0.51	0.45	0.37	0.43	0.39	0.33	0.24
M8	.3220	0.36	0.28	0.18	0.23	0.39	0.32	0.29	0.34	0.36	0.45

D.   TIME SERIES

Figure 13 shows the thermistor records from the Alpha Omega thermistors on the NB (green) and BB (blue) moorings with the sea level from the Monterey Bay tidal station

overlain. Initial inspection of Figure 13 immediately reveals the presence of periodic rapid temperature drops at both the NB and BB locations, separated by more gradual periods of warming. It appears that the temperature drops are due to the passing of an internal tidal bore from farther down-canyon, and will be discussed further.

The temperature drops at the two mooring locations have different characters (Figure 14). As seen on 09 August 1997, the BB records clearly shows two large temperature drops, whereas the NB record shows four smaller temperature drops. The difference in the two records may be due to the locations·of each mooring relative to the canyon topography. The MBARI bathymetry data indicates that the NB mooring was south of the canyon axis on a bank ~40 to 50 m above the floor of the canyon axis. The BB mooring appears to have been just off the center of the canyon axis. The actual locations of the two moorings made the BB mooring a natural selection for a more in-depth analysis.

THIS PAGE INTENTIONALLY LEFT BLANK

IV. DESCRIPTION OF THE TIDAL BORE

The most prominent signal in the BB mooring temperature and velocity records will be referred to a priori as that of a tidal bore. An accurate and reliable method to identify the passing of a bore was sought. It was found that the tilt values recorded by the ADCP pitch and roll sensors showed sudden changes that were highly correlated with the rapid temperature drops (Figure 15). It was also found that an increase in the up-canyon current accompanied the large tilt excursions and temperature drops, as shown for the pitch and near-bottom currents on 09 August 1997 (Figure 16). This figure shows the typical relationship among these three variables.

It seems unlikely that the mooring motion caused by the bore passage seriously contaminated the measured velocities. Any velocity oscillations at the period of the mooring motion are small (Figure 16) and there is no coherent high frequency signal throughout the water column that matches the period of the experienced tilts (Figure 21).

A. TIMING RELATIVE TO SEA LEVEL

The bore signal changes throughout the 34-day record (Figure 13). To investigate a possible relationship with the barotropic tidal signal, the timing of the bores relative to sea level as measured by the Monterey tide gauge

was examined. For the entire 34-d record, the onset of each bore was visually identified in the temperature record and the time difference between events was calculated. The time difference varied between 1 and 24 hours but in general fell between 10 and 14 hours with a mean of 11.9 h, slightly less than the period of the M2 constituent (12.42 h). The few time intervals exceeding the K1 period and the few extremely short intervals may result from errors in the visual reading of the temperature records.

During 01 to 09 September 1997, large signals in instrument tilt, near-bottom temperature, and near-bottom velocity occurred with great regularity. This time period was examined in more detail. The times of bore passages were estimated from the tilt records as the time when the angle of pitch exceeded ± 1°. Over these nine days, the bores had an average separation interval of 12.3 h, with a maximum of 13.4 h, a minimum of 11.3 h, and a standard deviation of 0.6 h. Over the same time period, the high tide had a mean interval of 12.3 h, a maximum of 13.4 h, a minimum of 11.4 h, and a standard deviation of 0.6 h (Figure 17). Over these nine days, the time interval between a bore passage at mooring BB and the previous high tide had a mean of 8.6 h with a maximum of 9.5 h, a minimum of 7.8 h, and a standard deviation of 0.6 h (Figure 18).

To examine the hypothesis that the temporal variation in the strength of the internal bores may be related to the spring/neap cycle, the ADCP pitch was used as a proxy for identifying the passage of the bores. The pitch record is compared to the tidal range, calculated as the range from either high tide to low tide or low tide to high tide, over the entire 34-day record (Figure 19). It is immediately obvious that two of the three sets of strong bores (~8/6-8/11 and ~9/1-9/9) occur when the tidal ranges are close to their minimum while only four strong bore signals occur during the three-day period when the tidal ranges are greatest (~8/16-8/19). From 21 to 24 August, when the tidal ranges are again near a minimum, only two strong bores are noted.

B. VERTICAL STRUCTURE

Since data from ~12-h time-series of CTD casts were available at the Shallow CTD station on 09 and 21 August 1997, these two days will be examined in more detail. These two observation periods seem to fall in different regimes for the bore. While a significant bore passed through this region of the canyon on 09 August, only weak, or no, bores were seen on 21 August.

1. 09 August 1997

Figure 20 shows all of the density profiles derived from the CTD casts conducted at ~30-min intervals at the

Shallow CTD station from 0708Z until 1848Z. In addition, the average density profile and the N^2 profile calculated from it (using Δz of 1 m) are also shown. Perhaps the most notable feature in this figure is the sharp pycnocline. At ~200 to 250 m depth, near the depth of the upper bins from the moored ADCP, the temporal variance is much larger than near the bottom.

Figure 21 shows the BB and vessel-mounted ADCP total speed data (both 1 min and 3 min), isopycnal depths derived from the CTD data, and the temperature data from the moored Alpha Omega thermistor during the time period of the CTD station. This figure shows that CTD casts began shortly after the passing of a bore and end shortly before the start of the next bore. The internal tide signal is clearly seen in both the moored ADCP records and the vessel mounted ADCP records, showing a reasonable match at the interface between the two measurements. Figure 22 is a plot of the east and north currents from the BB ADCP at a depth of 217 m and from the vessel mounted ADCP at a depth of 215 m. The two ADCP's show better correlation in the phase than in the magnitude of the currents. This difference is attributed to the spatial offset of over 1-km between the BB ADCP and the location of the CTD casts. Even though the vessel mounted ADCP was not directly over the BB mooring, it was mainly over the canyon axis farther down canyon. Given the

vessel's location, if the bore affected the upper water column, some evidence of an offset bore passage should be seen in the vessel mounted ADCP record. As seen in Figure 21, there is no evidence for bore effects above 209 m.

The first bore on this day, seen at ~0700, is shown in detail in Figure 24. It is easier to see in this figure how the CTD casts begin shortly after the commencement of the 0700 bore. This particular bore is associated with one of the largest temperature drops recorded during the entire 34-day record. The initial temperature drop for this bore is ~0.5° C in 1 min. The maximum range for this bore is ~-1.25° C in 11 min. The initial drop is 40% of the final temperature decrease and occurs over just one sampling interval of the thermistor. Maximum current speeds close to the bottom are up-canyon in the 45 to 55 cm/s range and occur within 30 min of initial temperature drop. Currents accelerated in the up-canyon direction with a maximum value, ~0.24 cm/s^2, at 12 m above the bottom coincident with the time of the initial temperature drops. Starting at ~0730, thin "finger-like" regions of increased current speed extending upward 80 to 90 m from the bottom are present for ~20 min. A maximum recorded current of 69 cm/s occurred ~40 m above the bottom (bin #8, 32 m above the transducer) approximately 35 min after the initial passing of the bore. These high velocity events in time and depth are associated

with current relaxations between the short current pulses higher in the water column. Figure 23 shows that the current actually relaxes rather than totally reversing between each of the high velocity events.

The second bore on 09 August occurred at ~1845 and has similar velocity structure as the first (Figure 25). The temperature signal for this event is not as clear. The maximum temperature drop associated with this bore is 1° C in 50 min with a maximum single step of just 0.25° C occurring near the end of the temperature drop. This single step represents 25% of the total temperature range. The maximum current speeds near the bottom are in the same range as the earlier bore (45 to 55 cm/s) and occur with the same timing (within 30 min of initial temperature drop). However, this bore lacks the high-speed current pulse seen in the earlier bore at 40 m above the bottom. The maximum acceleration seen at 12 m above the bottom is ~0.12 cm/s^2 approximately 60 min after initial bore passage, and does not occur at the time of initial bore passage which has an acceleration of ~0.1 cm/s^2. The "finger-like" structures above this bore are more uniform in time and space and they are easier to identify than in the earlier bore.

In addition to the signal associated with the two temperature drops, a series of pulses of high speed flow (~50 cm/s) occurs ~60 m above the bottom between 250 m and

270 m depth from ~1400 until ~1800 (Figure 26). These strong pulses enhance the generally down-canyon flow occurring during this time period. The pulses occur with an average period of 2.5 min and gradually increase in strength over 60 min before dying away. The period of these pulses is longer than the period of the buoyancy oscillations (~1 min) at these depths, making it possible for these oscillations to be freely propagating internal waves, perhaps generated from a small ridge or other topographic feature up-canyon of the BB mooring site and advected down-canyon by the lower frequency background flow.

2. 21 August 1997

Figure 27 shows the density profiles calculated from the CTD casts conducted at the Shallow CTD station from 1029 until 2140 on 21 August 1997. The difference in density structure between 21 August (Figure 27) and 09 August (Figure 20) is immediately apparent. The water column is more continuously stratified on 21 August and the pycnocline much less distinguishable. In fact, comparison with the data collected at the deep CTD station indicates that much of the change took place between 09 and 10 August. Buoy measurements indicated that winds reversed from equatorward to poleward on 07 or 08 August (depending on location), and HF radar-derived surface currents across the mouth of Monterey Bay show a similar reversal on 08 August. While cloud cover limited availability of AVHRR data between 08

43

and 11 August, the 07 August image shows the characteristic upwelling pattern, whereas 12 August is uniformly warm. Winds are again equatorward, although not particularly strong, during 12 to 15 August, followed by a weak relaxation during 16 to 18 August. Surface temperatures are high throughout this period. Previous work (Rosenfeld *et al.* 1994, Ramp *et al.* 1997) has shown that a warm meander, of significant vertical extent, moves shoreward into the bay during relaxations of the upwelling-favorable winds typical for this time of year. The observed changes in stratification could well be due to such a mesoscale event. Earlier observations of this phenomena would indicate that the density adjustments take place within one day of the changes in the winds, whereas an interval of at least two days must have elapsed if this mechanism is responsible for the changes observed in these data.

Figure 28 is a contour plot of the moored ADCP data from 21 August. Unfortunately, the shipboard ADCP was experiencing difficulties on that day making full water column measurements impossible. However, since on 09 August when a particularly strong bore was noted, the effects did not extend above 209 m, it is reasonable to assume that not much of the signal of interest is missed by not having VM-ADCP data on 21 August when the bore appears much weaker. On this day CTD casts began between bores and continued through the passing of a bore at ~1345. CTD casts continued

44

well after the bore's passage and ended between bores with the velocity and density structure in much the same state as when they began. Figure 30 shows the velocity vectors from the BB ADCP.

The temperature drop associated with this bore is very weak, taking just over 2.5 h to fall 1° C with the maximum single jump of just 0.05° C in 1 min (5% of total temperature drop). The maximum current speed 12 mab is 44 cm/s, as compared to 55 cm/s in the 0700 bore of 09 August (Figure 29). It occurs ~45 min after the temperature starts to drop. The maximum acceleration at 12 m above the bottom is ~0.05 cm/s^2 and does not occur at the time of initial bore passage which has an acceleration of ~0.03 cm/s^2. These accelerations are barely distinguishable from the background flow, which has accelerations from 0.01 to 0.03 cm/s^2. The ADCP tilt records show little activity in response to this bore (Figure 15). Although the tidal bores on 21 August are significantly weaker than on 09 August, their vertical structure is similar.

THIS PAGE INTENTIONALLY LEFT BLANK

V. DISCUSSION

The kinetic energy in the internal wave band in the Monterey Canyon is widely distributed among tidal constituents. These include several of the shallow water constituents that are a result of the non-linear interactions of the internal tide with the ocean bottom (Werner 1992). As shown in Figure 11, the energy is more concentrated at the M2 frequency higher in the water column and spreads out more into the overtides as the bottom is approached. Sharp temperature fronts and strongly bottom-intensified velocity signals occur approximately at 12-h intervals. The time interval between bores, averaging 11.9 h over the whole 34-d period and 12.3 h during 01 to 09 September, does not exactly match that of the M2 constituent (12.42 h) nor does it maintain a constant relationship to the maxima in sea level, indicating that a mix of factors comes into play. It is not clear where and how these features form, why they vary in strength over the 34-d record, and what dynamics control them.

We have described the bottom-intensified signal as an up-canyon propagating internal bore rather than as a soliton train. These two seemingly different non-linear phenomena can be thought of as a continuum (Munk 1981, Ostrovsky and Stepanyants 1989), an initial disturbance that becomes bottom-intensified through critical reflection (Thorpe

47

1992), steepening of the wave front into a bore, and finally evolving into a soliton train (Ostrovsky and Stepanyants 1989) that breaks in the shallow waters near the canyon head. To identify where in the continuum the events described in this thesis lay, the characteristics of each stage in the evolution were compared to our observations.

Evidence to support the claim that the events described here have fully evolved into a soliton train could not be found. First, solitons have usually been observed on a density interface near the surface or mid-water column (Ostrovsky and Stepanyants 1989, Stanton and Ostrovsky 1998), and on occasion near the bottom in highly stratified water (Bogucki *et al*. 1997, Holloway 1987). The events described here occur near the bottom in weakly stratified flow. Second, fully developed soliton trains exhibit a rank ordered structure (Ostrovsky and Stepanyants 1989) that is not clearly present in our data. Third, the stronger events described in this thesis are associated with strong up-canyon current accelerations and temperature drops that indicate a frontal passage, leaving the fluid in an altered state, rather than the temporary changes wrought by a soliton. For these reasons and the analogy with tidal bores on rivers, these events should be regarded as internal bores rather than as a train of solitons. Ultimately, bores and solitons are closely linked and can be thought of as steps in the evolution of linear internal waves to turbulence.

48

The finger-like projections of high velocity current extending above the bottom layer could be turbulence, high frequency internal waves, or even solitons associated with the bore front, but without downstream measurements to record their evolution and higher temporal resolution measurments this remains unresolved.

A.   BORE FORMATION

Two types of scenarios leading to the generation of internal bores have been proposed. One, inspired by Halpern's (1971) observations in Massachusetts Bay, consists of three phases: formation of an internal front due to blocking of the stratified flow by a topographic feature, non-linear steepening of the front, and the formation of new waves due to the interaction of dispersion and non-linearity (Lee and Beardsley 1974). The second involves steepening of a large amplitude internal tide as it shoals (Holloway 1987). Either, or both, of these mechanisms could be at work in generating the bores described here.

Petruncio *et al.* (1998) have previously shown the presence of a large amplitude internal tide in Monterey Canyon due to energy concentration by the near-critical sloping bottom and the narrowing canyon walls. Furthermore, based on their observations made well above the bottom boundary, which compared well with linear theory, they suggested that the Monterey Canyon internal tide is

generated outside the confines of Monterey Bay. They proposed two possible generation sites based on characteristic ray tracing of the M2 constituent. In identifying these sites, they assumed that while the internal tide may be steered by the canyon, the signal would not propagate through the numerous sharp bends and curves in the canyon bathymetry without significant modification, and so the internal wave they observed was likely generated in a wedge defined by the north and south wall orientation at the canyon head. Data presented in this thesis, from an area near a tight bend in the canyon, show that strong non-linearities of the internal tide may be associated with small-scale topographic features.

Holloway (1987) examined a series of bores propagating onto the Australian North West shelf, and using the assumption of two-layer flow, was able to describe the conditions required for their formation using Froude numbers. The Froude number for a particular layer can be calculated using equation (23) and the critical Froude number for a bore to form can be calculated using equation (24) with appropriate adjustments for the lower versus upper layer. The situation observed near the bottom of Monterey Canyon does not easily lend itself to analysis in terms of layers, nor is it possible with measurements at one fixed location to determine the speed of the bore since the measured velocities are a combination of the flow relative

50

to the hydraulic jump and the motion of the jump itself. While theoretically over a flat bottom with layered flow, a bore could be moving in either direction, while still registering up-canyon flow coincident with temperature drops, in stratified flow over the sloping bottom an up-canyon-propagating bore seems much more likely (Figure 31). Conceptually, the analogy with a bore propagating upriver is very appealing, but further analysis is needed to see if the conditions necessary for a hydraulic jump can be verified.

B. TEMPORAL VARIABILITY

While the strength and occurrence of the internal bores show considerable temporal variability over the 34-d record considered here, there is no clear correspondence to the spring/neap cycle of the barotropic tide (Figure 19). The most regular bore passages occur during the neap phase at the end of the record, while an earlier neap phase does not show a clear bore signal. Clear bore signals are also seen during the first spring phase of the 34-d record while the second spring phase, with slightly smaller sea level ranges, has no clear bore signal. During the 01 to 09 September time period, when the bores are consistently strong and regular, they are phase locked (to within 1 h) to the sea level (Figure 18). In Figure 32, the 1026 kg/m^3 isopycnal is taken to represent the background density field of the internal tide and the 1026.5 kg/m^3 isopycnal is taken to

51

represent the isopycnal displacement of the internal bore. In these two cases, the background signal is phase locked to the sea level but the bore signal can be clearly seen out of phase with the background on 21 August (weak bottom intensification), and in phase on 09 August (strong bore). From this we can infer that strong bores will occur approximately 8.6 h after high tide when conditions are conducive to bore formation.

C.   RECOMMENDATIONS AND IMPLICATIONS

This thesis presents an initial description of some of the most notable features in the moored data from the Monterey Canyon internal wave experiment. There are still a number of unresolved issues however, including whether it can be determined to a high degree of certainty that what has been described here is in fact an internal bore. Secondly, while some intriguing connections between the background stratification and the strength and regularity of the bores have been noted, the dynamical reasons for this have yet to be worked out. Furthermore, the cause of the finger-like current pulses is unresolved. Also, the high frequency pulses that are moving down-canyon on 09 August have not been addressed in any detail. It is possible that they are internal waves formed by some topographic feature farther up-canyon, but the question remains as to why they are not seen every time there is down-canyon flow. Both of

these phenomena could be better explained by taking new measurements that have higher temporal and spatial resolution. An experiment that included continuous density measurements throughout the water column at several locations along the canyon axis would add insight into the development, propagation and evolution of the bores. Simultaneous sampling over a large section of the canyon would require numerous moorings and instruments, probably a cost-prohibitive exercise, but successive deployments in various areas farther down-canyon from the experiment site discussed in this thesis could accomplish many of the same goals.

Even without a clear understanding of the formation and dynamics of the Monterey Canyon bores, the effects they have on measurements and operations in and around the canyon can be planned for. Several oceanographic institutions are located near Monterey Bay that conduct research in the canyon. One in particular, MBARI, uses ROV's to explore the canyon and is beginning to experiment with AUV's as well. Understanding and being able to predict the presence of strong internal bores can benefit these operations by reducing the risk of possible equipment loss. As recently as September 1999, an AUV was lost in the canyon possibly due to interference caused by an internal bore overtaking the vehicle. The effects of the bores can cause difficulties in operating in canyons beyond the threat of

undesired motion. The bores are capable of resuspending a significant amount of sediment as they propagate up the canyon (Bogucki *et al.* 1997), significantly reducing visibility. Canyons also have a rectifying effect on the tidal currents in them (Lafuente *et al.* 1999) that can have the effect of bringing deep waters onto the shelf. Mixing associated with strong internal wave motions may also introduce high nutrient concentrations into the euphotic zone, thus enhancing productivity.

VI. CONCLUSIONS

Thirty-four day records of near-bottom temperature and horizontal velocity throughout the lower third of the water column from within Monterey Canyon were examined. The internal tide was found to be highly non-linear with kinetic energy dispersed among numerous overtides near the bottom. Higher in the water column, energy is more concentrated into the primary semi-diurnal constituent, M2. Strongly bottom-intensified up-canyon currents were observed. The bottom currents and temperature varied in strength over the 34-d record, taking on the characteristics of an internal bore when they were at their strongest. Large up-canyon acceleration was accompanied by a rapid temperature drop. Figure 31 is a conceptualization of the internal bore that sometimes occurs at ~12-h intervals.

When strong bores are present, they are nearly phase locked to the sea level variations and arrive at the measurement site about 8.6 h after the high tide at Monterey. They have maximum currents of ~55 cm/s with speeds exceeding 30 cm/s over a duration of approximately two hours. They are evident in the velocity record up to at least 35 m above the bottom, and may be accompanied by high frequency pulses extending even higher. Temperature drops of up to 0.75° C in 1-2 min occur simultaneously with the

maximum acceleration (~ 0.24 cm/s^2) signaling the bore arrival.

The variation in the strength of the bottom-intensified currents is not caused by direct forcing from the tidal range like tidal bores on rivers (Pugh 1987), as the strongest bores do not occur during the spring phase of the spring/neap cycle. However, neither can it be said that the strongest bores will always be found during the neap phase of the cycle, even though that is the case during one portion of the records. Speculation on the reason for the strong variability observed in the strength of the bottom currents and the presence or absence of a bore centers on the stratification and the background shear in the mid-water column. The stratification on 09 and 21 August, days on which bores were present and absent, respectively, shows large differences. The mid- and deep water isopycnals oscillated in phase on the 9th and out of phase on the 21st, much as was observed by Petruncio *et al*. (1998) on two days in April and October 1994. Changes in the background stratification, perhaps caused by mesoscale events, could cause conditions more or less favorable to bore formation by changing the internal tide generation site and/or interactions with the background flow that would affect the strength of the internal wave and degree of wave steepening, a precursor to bore formation.
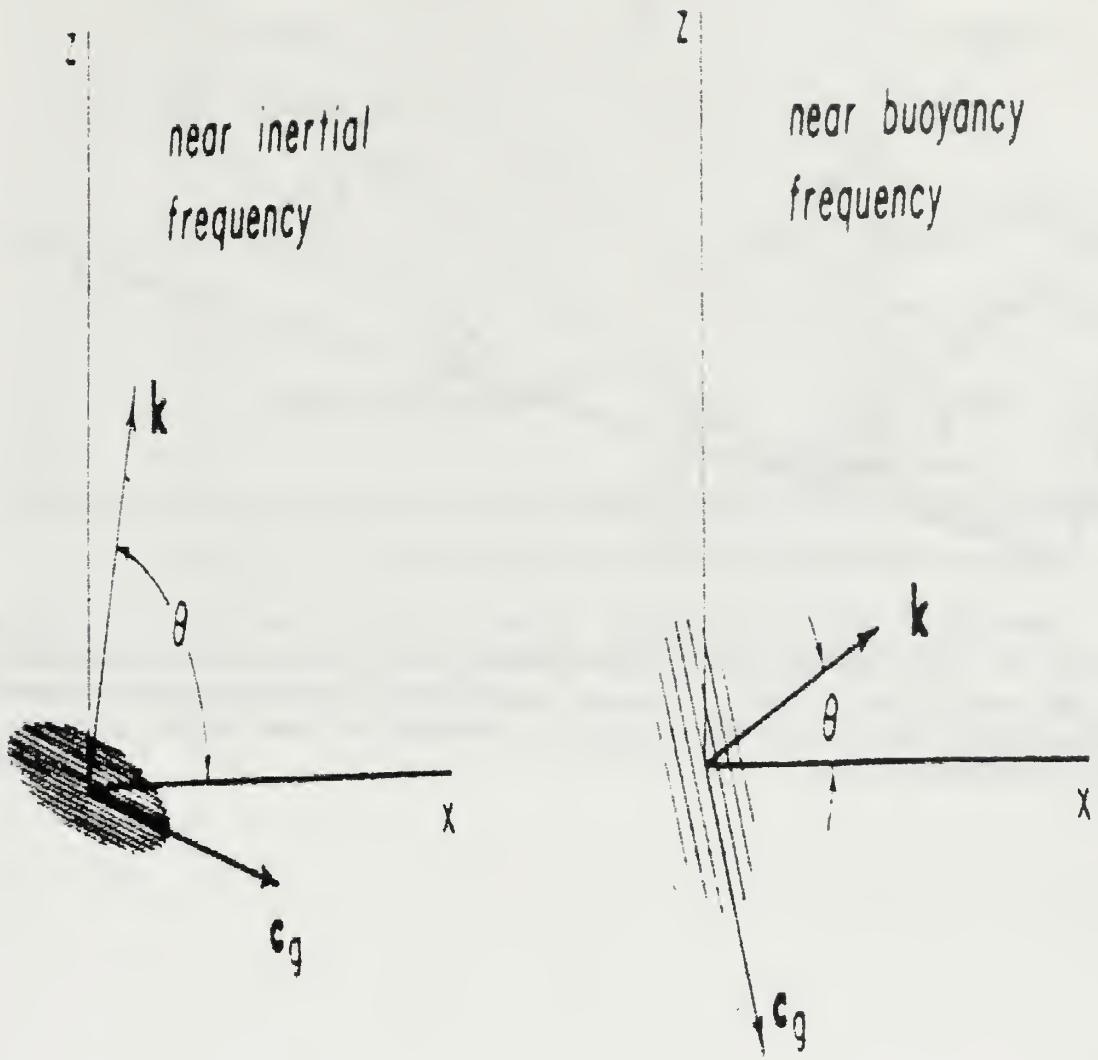
Figure 1. Visualization of internal wave propagation; phase and group velocities are along vectors $\bar{k}$ and $\vec{C}_g$, respectively (Munk 1981).
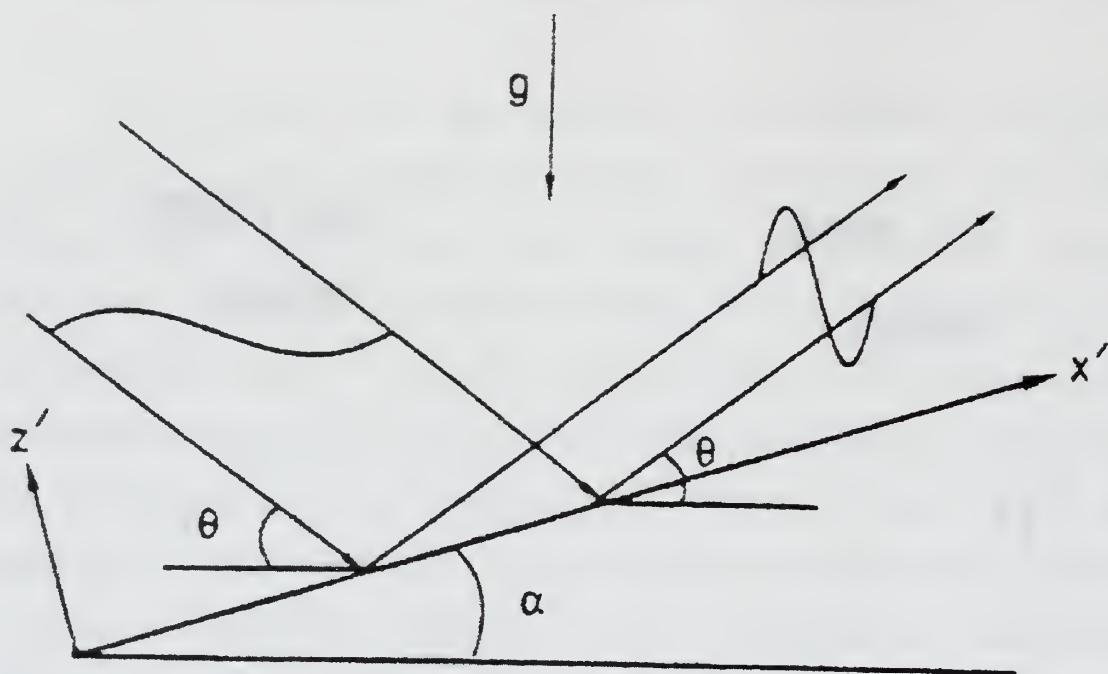
Figure 2. Illustration of internal wave reflection geometry (Slinn and Riley 1996), θ here refers to the angle of energy propagation while in the text it refers to the angle of phase propagation.
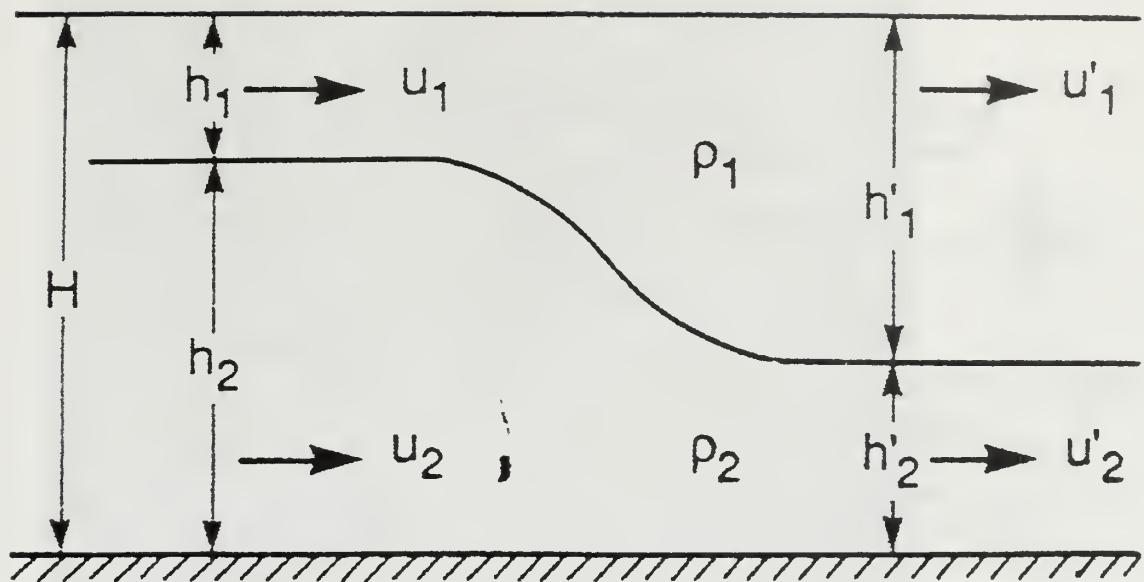
Figure 3.   Diagram of a 2-layer hydraulic jump (Holloway 1987).   This model can describe either a stationary or a propagating hydraulic jump.
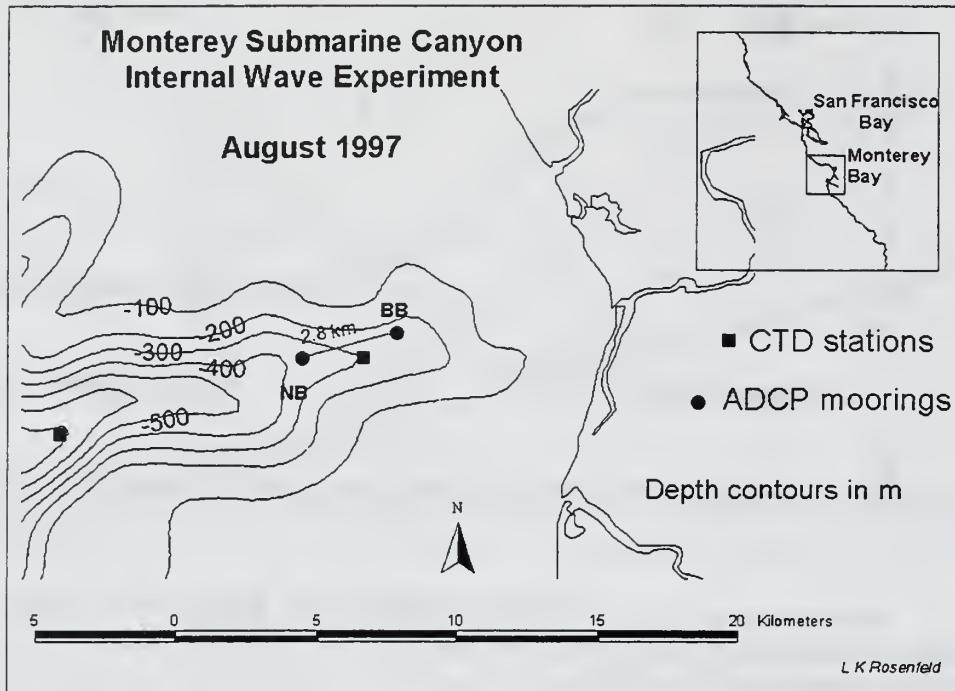
Figure 4. Experiment map. CTD station between the two moorings is referred to as "Shallow", other CTD station as "Deep".
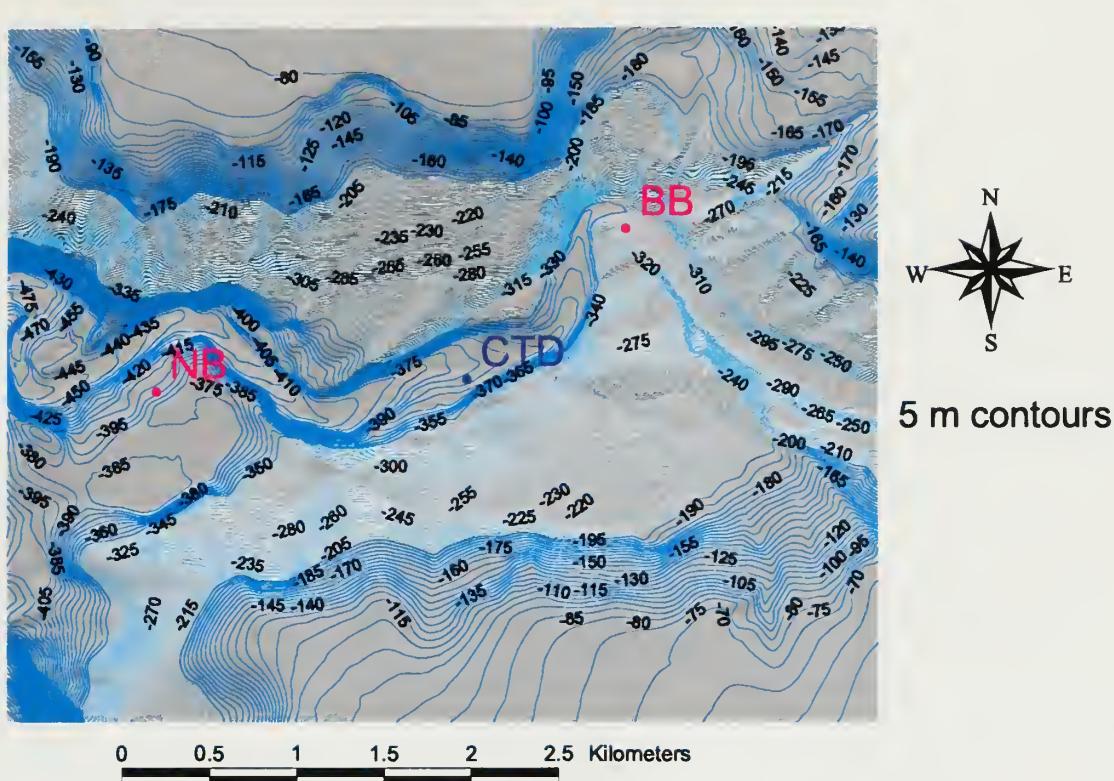
Figure 5. High-resolution bathymetry data from MBARI showing locations of NB and BB relative to the canyon axis.
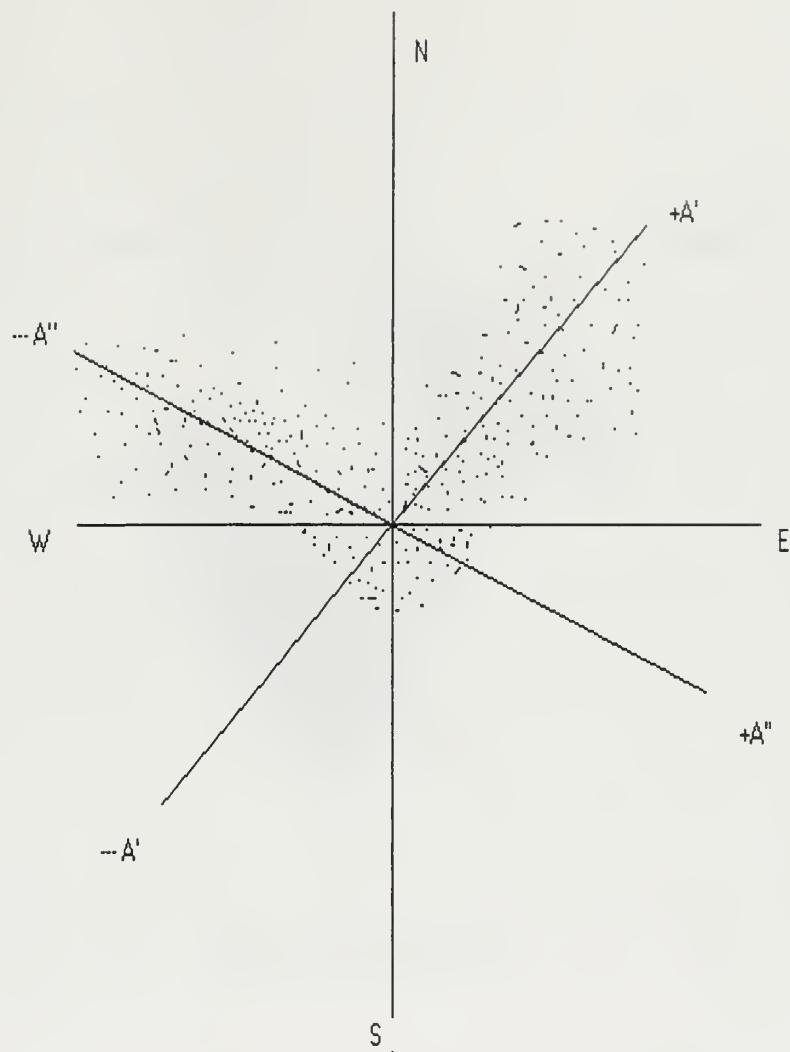
Figure 6. Concept for calculating principal axes for
current data. +A' is considered up-canyon and -A" is
considered down-canyon.
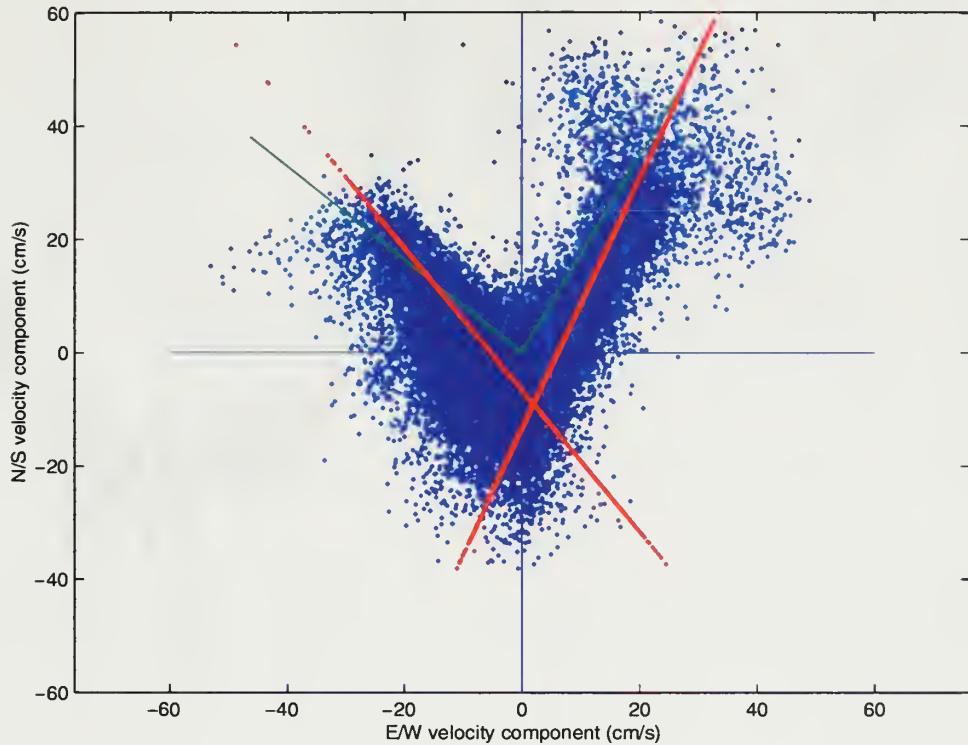
Figure 7. Current data from BB ADCP bin #1 (blue) with the derived principal axes from method one (green) and method two (red) overlain.
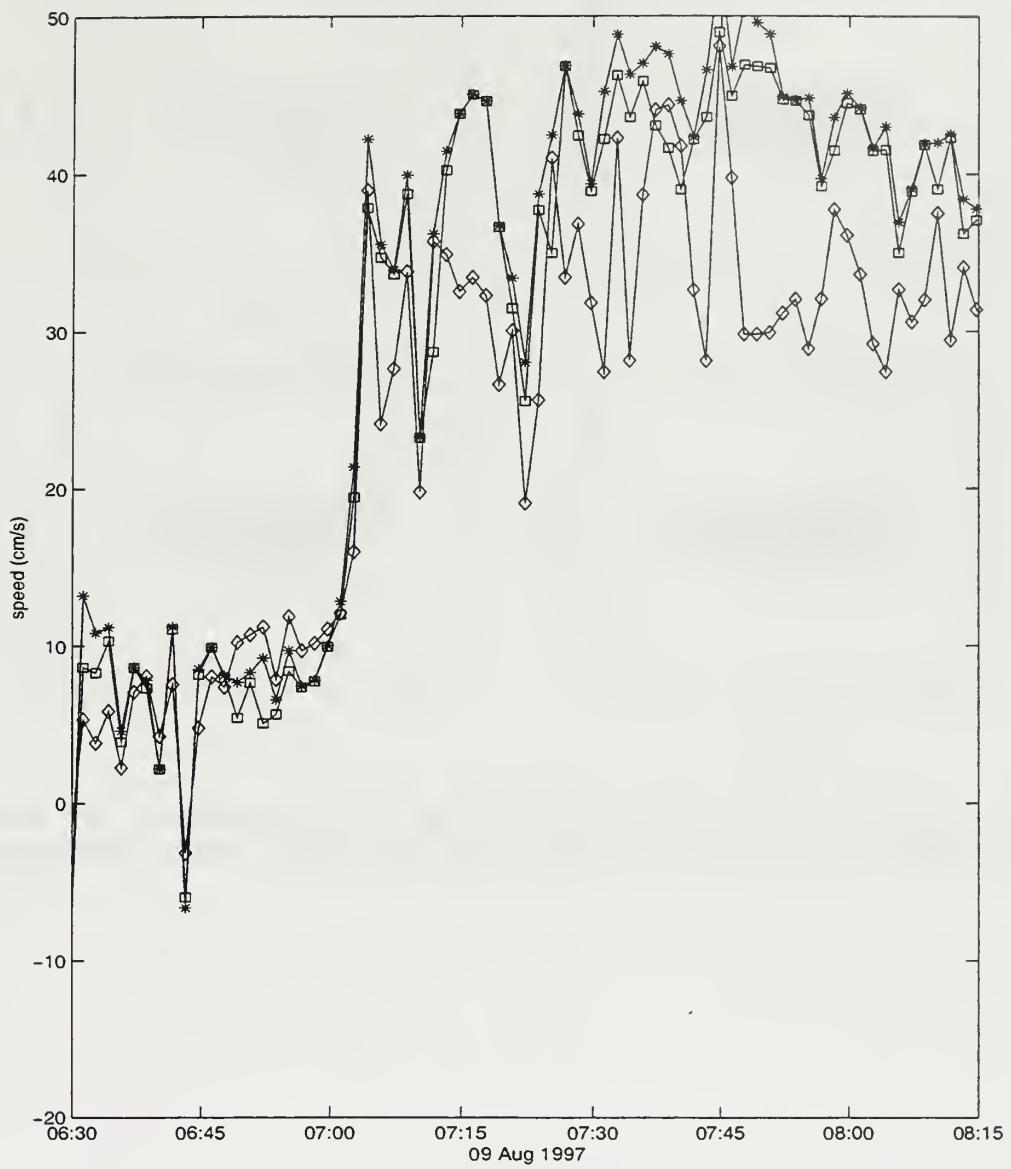
Figure 8. Comparison of BB ADCP bin #1 speed data (*) with method one speed (square) and method two speed (diamond). Where negative values indicate westward or down-canyon flow.
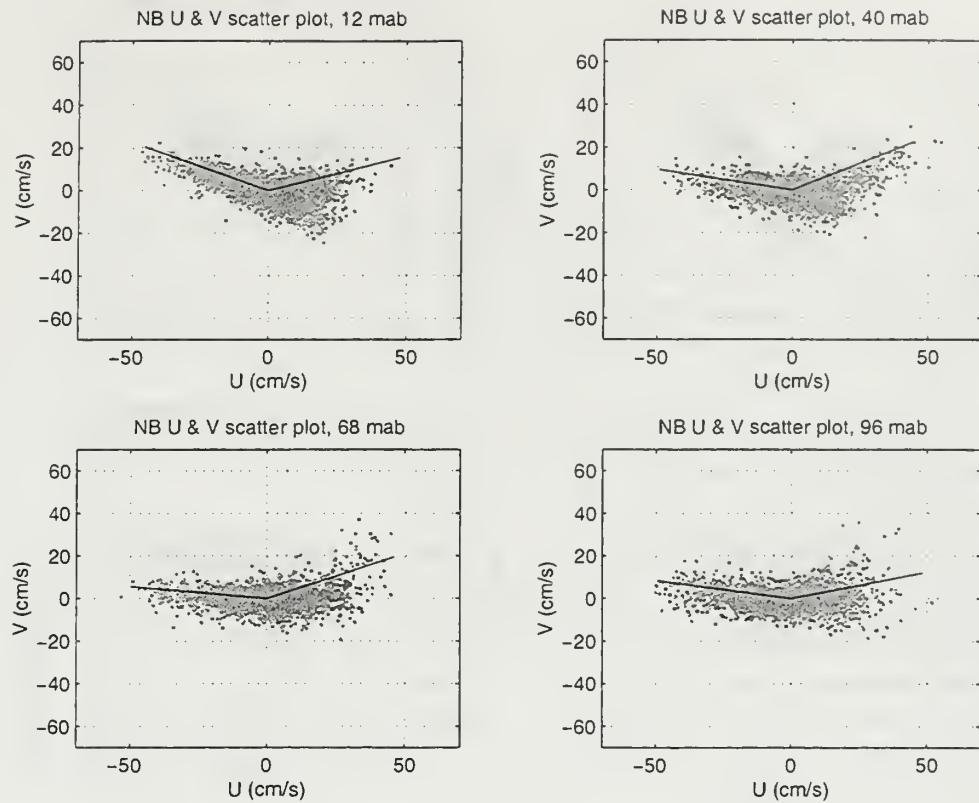
Figure 9. Scatter plots of NB ADCP velocities with up- and down-canyon axes drawn in for 12,40,68, and 96 m above the bottom.
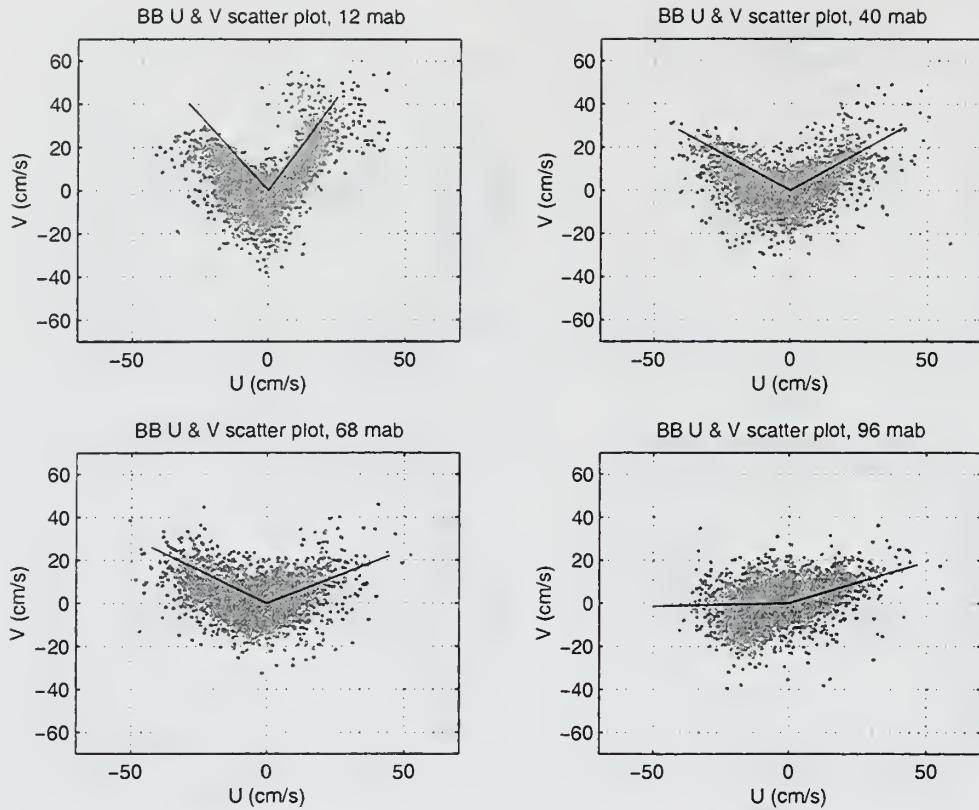
Figure 10. Same as Figure 9 except for BB ADCP.
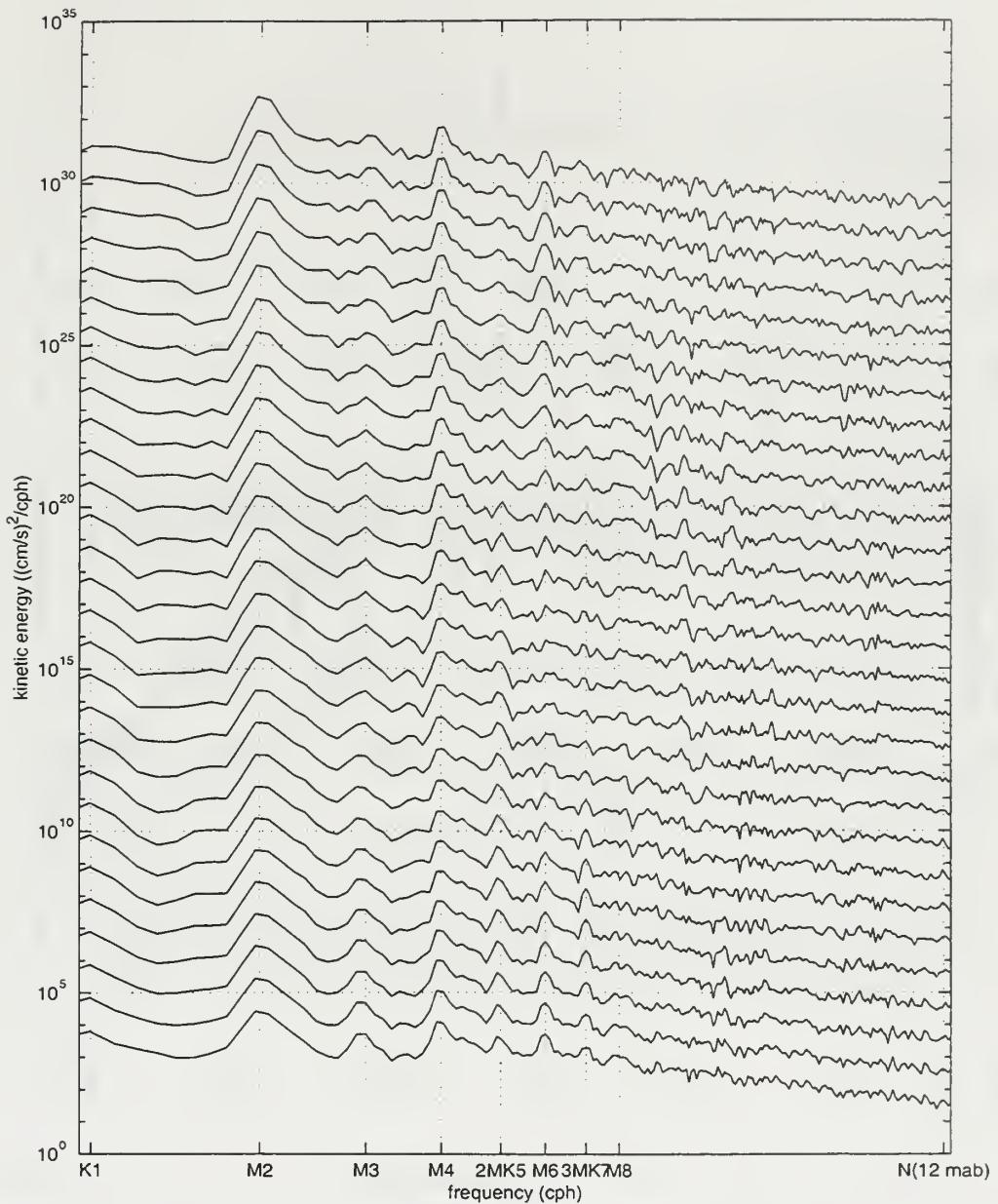
Figure 11. Kinetic energy spectrum for each BB ADCP bin, with successive bins offset by one decade. The position of several tidal constituents and the Brunt-Väisälä frequency 12 m above the bottom are indicated on the x-axis.
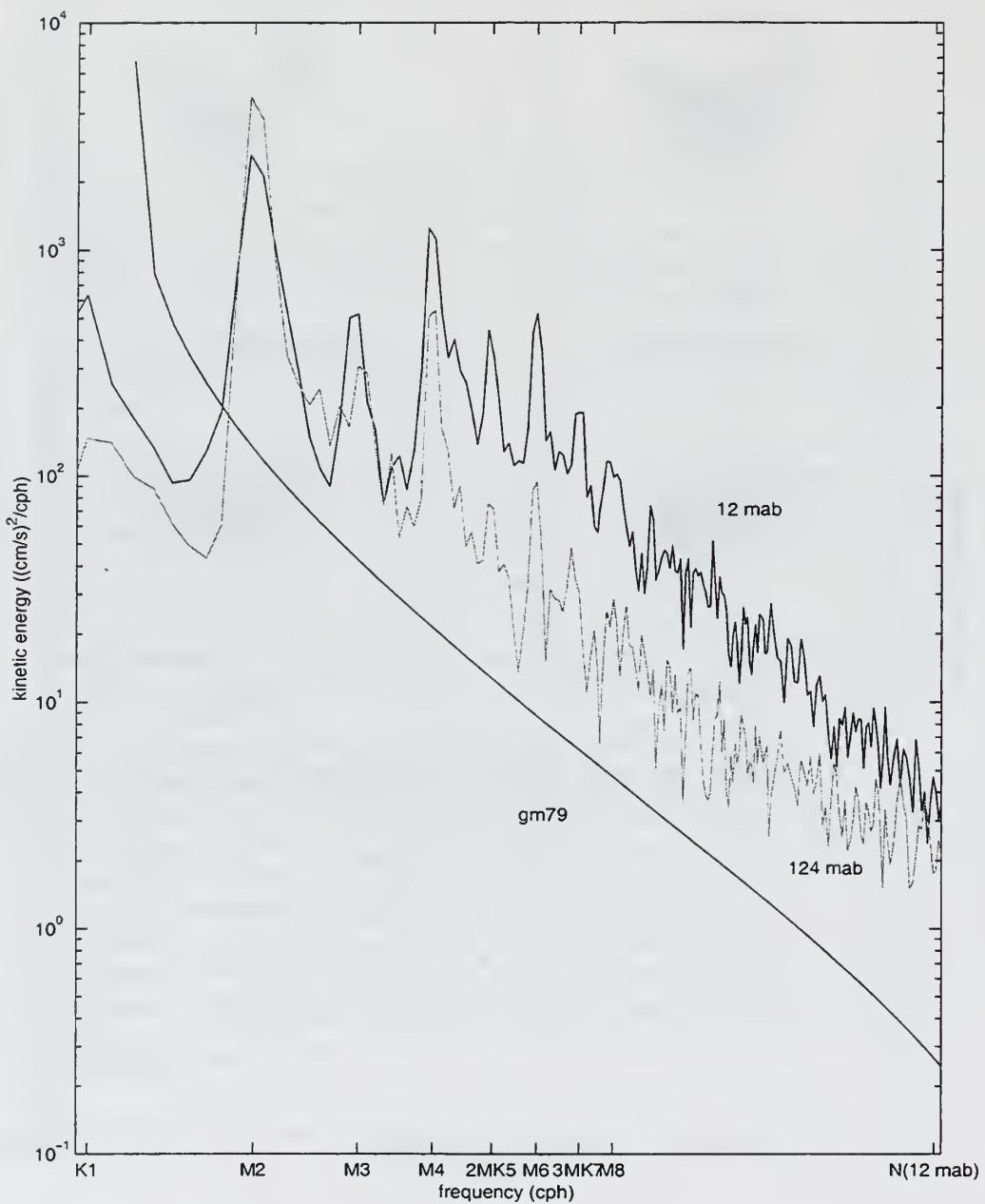
Figure 12. Kinetic energy spectrum from the near-bottom (12 mab) and middle water column (124 mab) showing intensification compared to the GM79 open ocean internal wave kinetic energy spectrum.
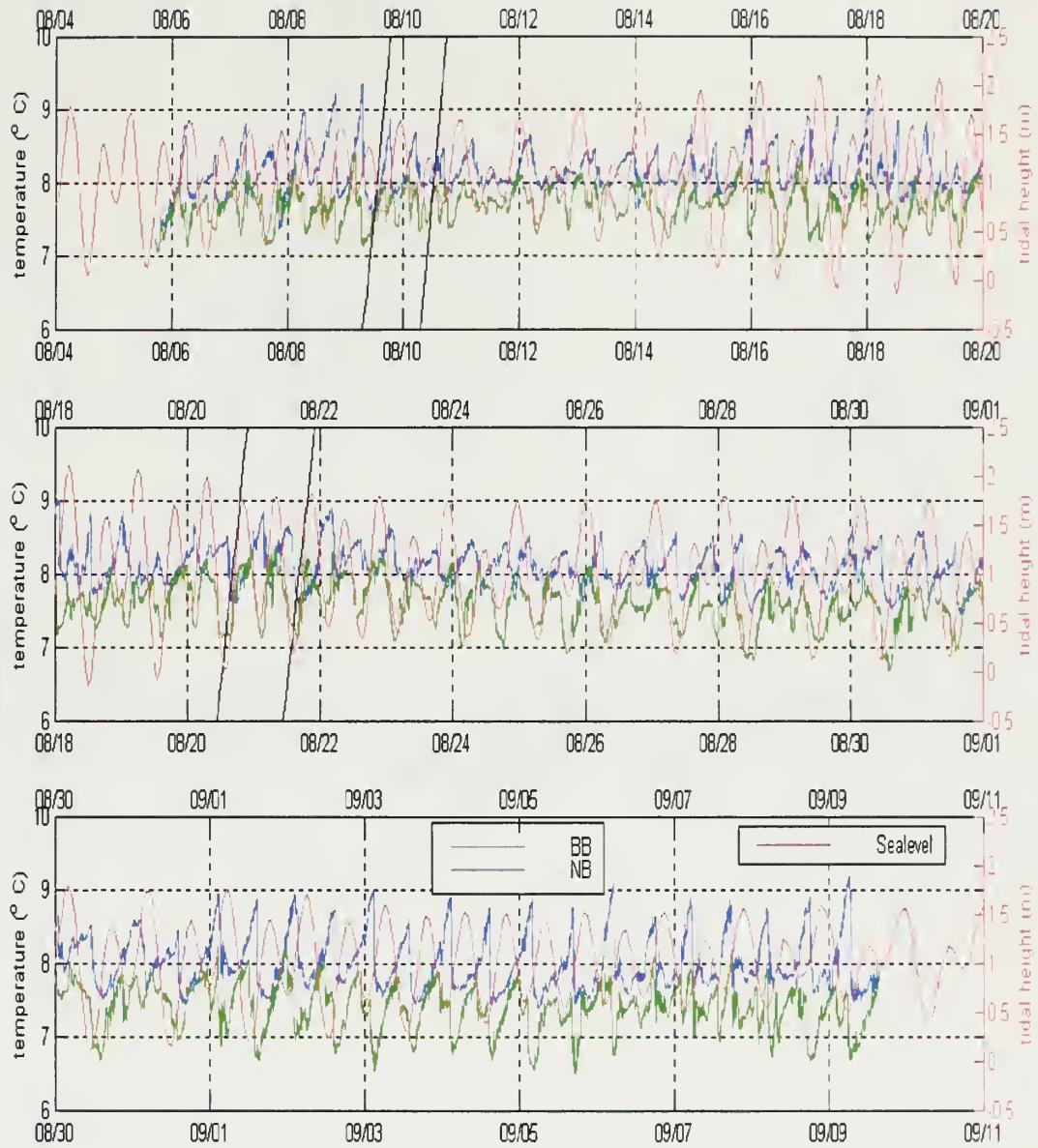
Figure 13. BB and NB temperatures with Monterey sea level
data overlain (05 August 97 - 10 September 97). The four
black slanted lines indicate the times of the four CTD time
series.
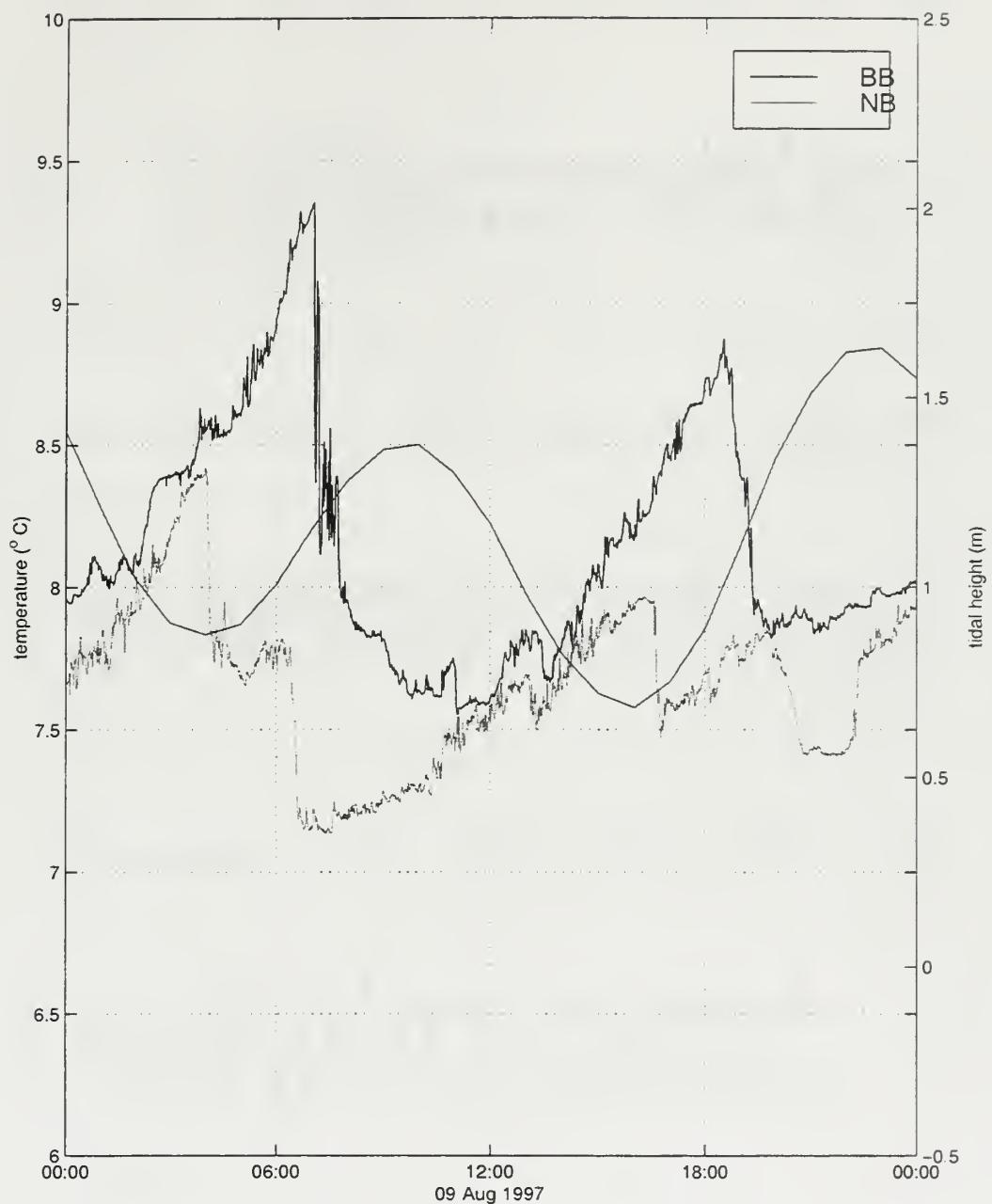
Figure 14. Alpha Omega thermistor records, BB (black) and NB (gray) with Monterey sea level overlain for 09 August 1997.
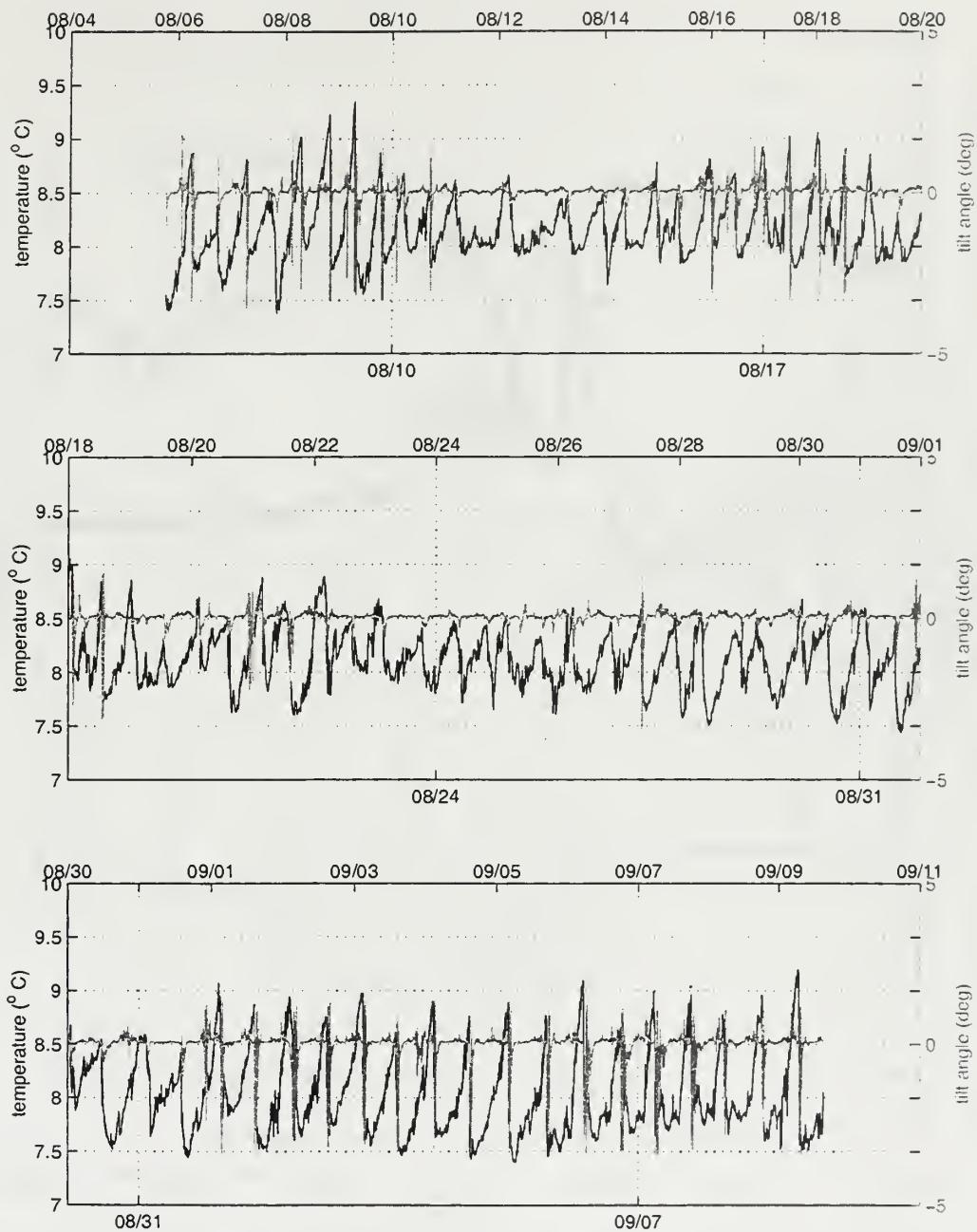
Figure 15. BB Alpha Omega thermistor and ADCP pitch sensor records.
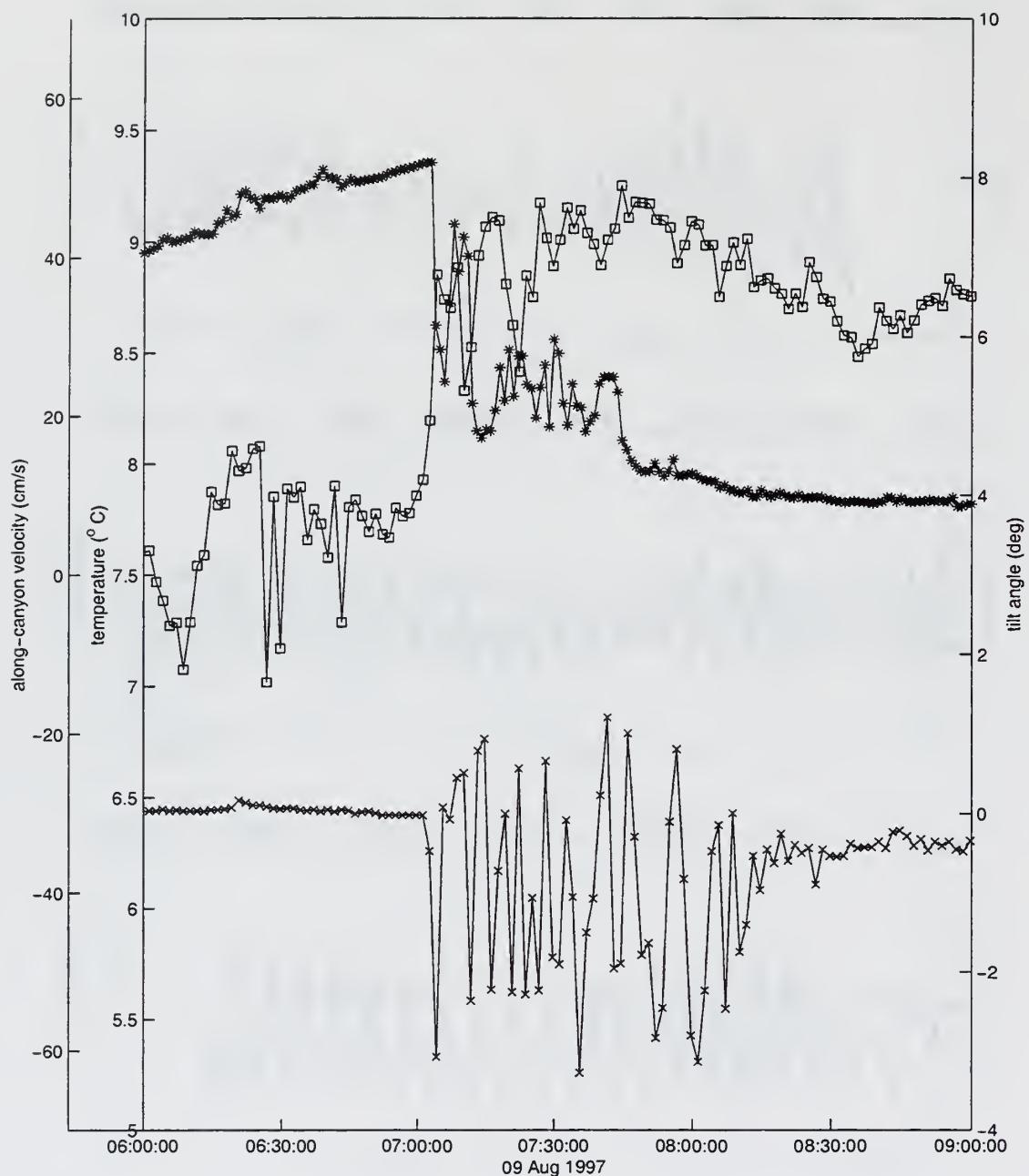
Figure 16. BB ADCP pitch sensor (X), along-canyon velocity (squares), and Alpha Omega thermistor (*) on 09 August 1997 showing bore passage.
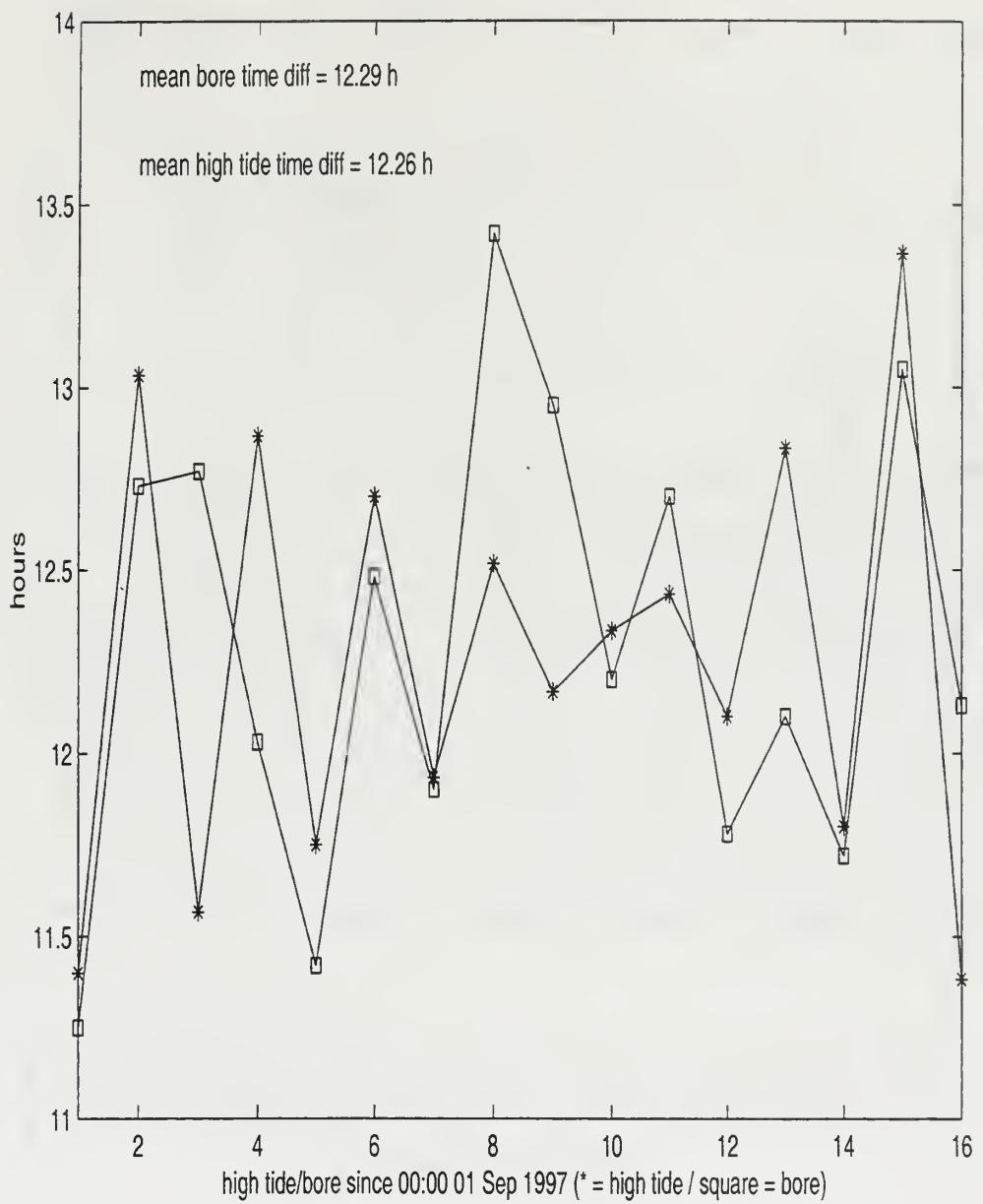
Figure 17. Differences between successive high tides and internal bores (01 to 09 September 1997).
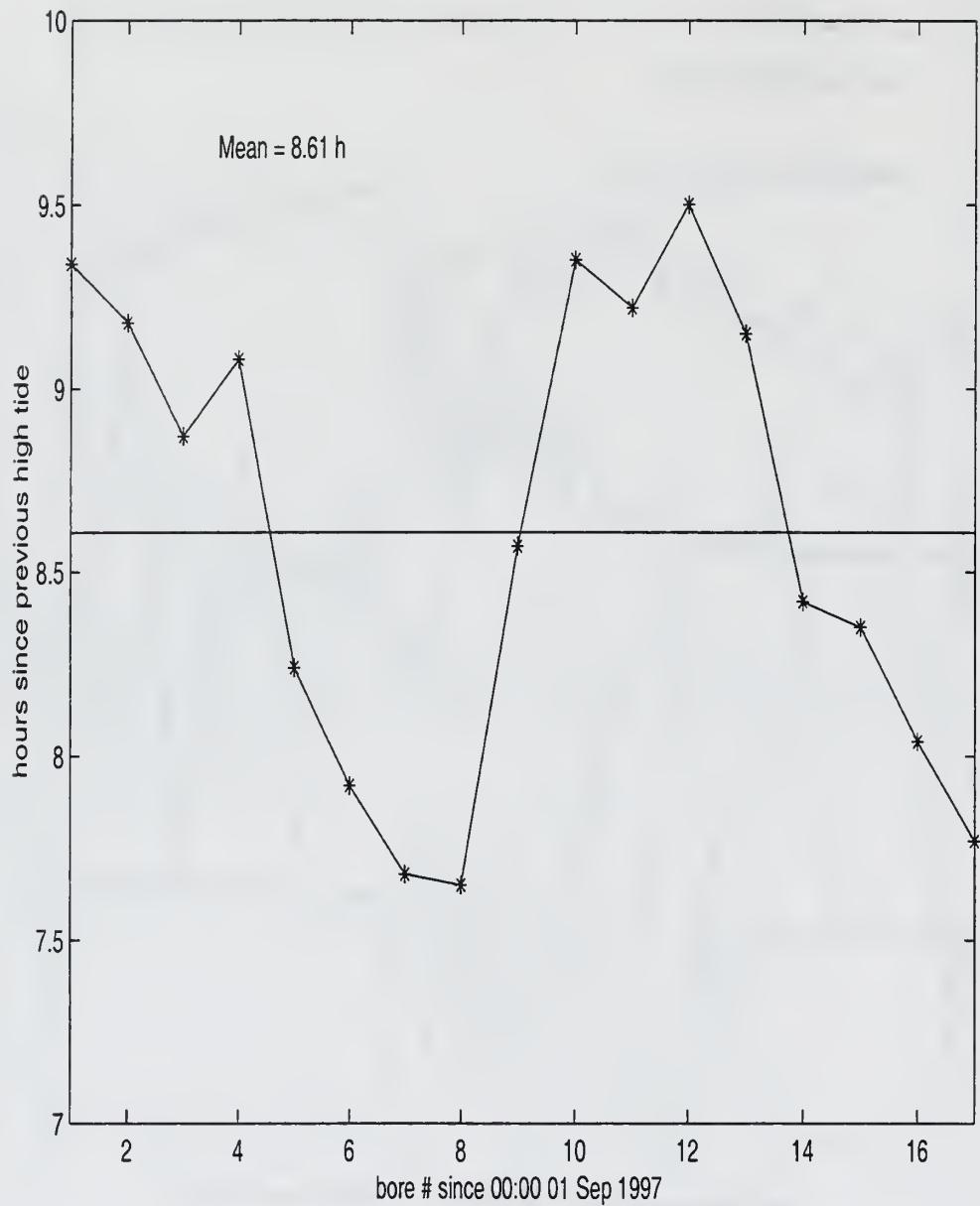
Figure 18. Time delay of internal bore passage relative to previous high tide.
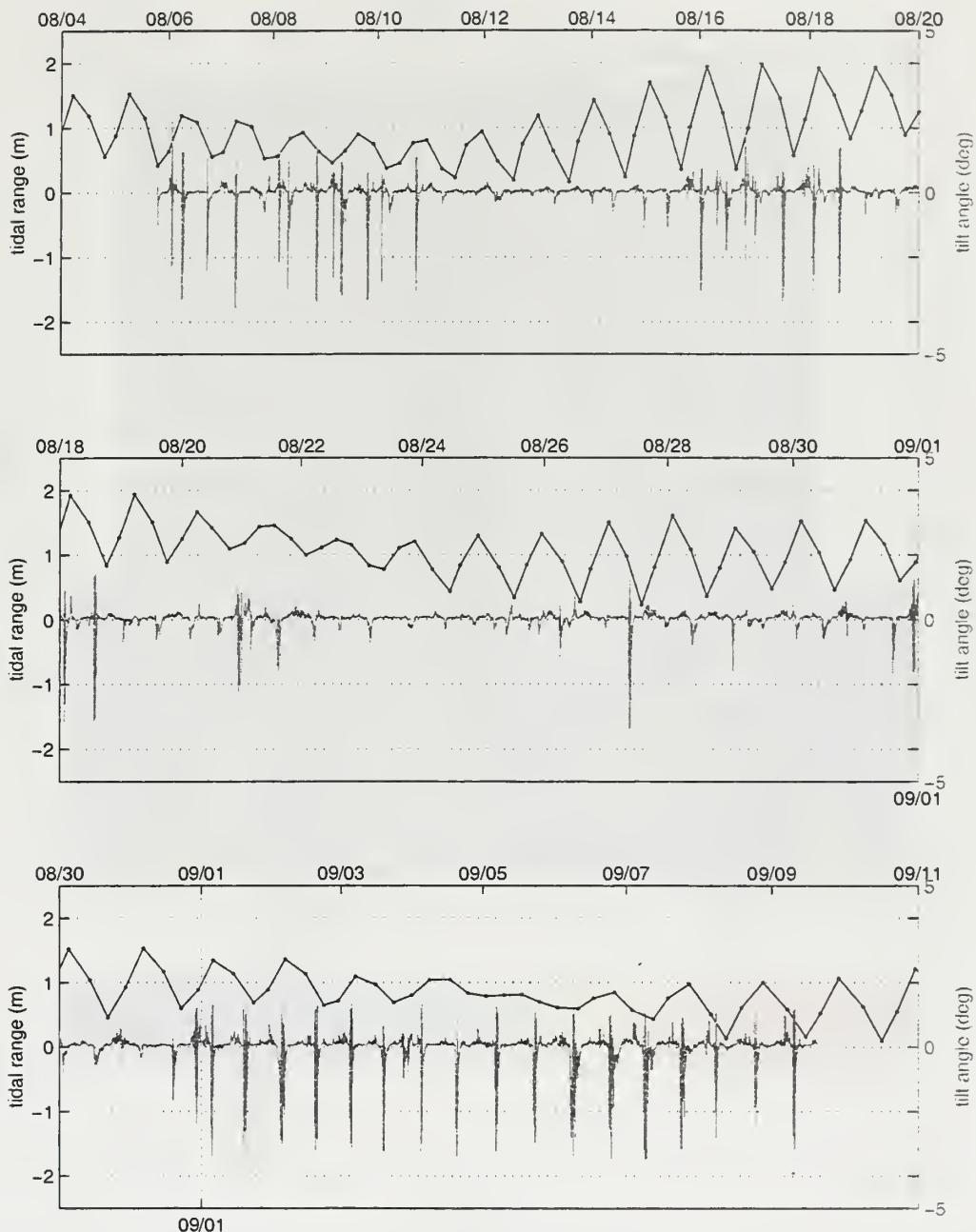
Figure 19. Sea Level ranges (black) and BB ADCP pitch
sensor (gray).
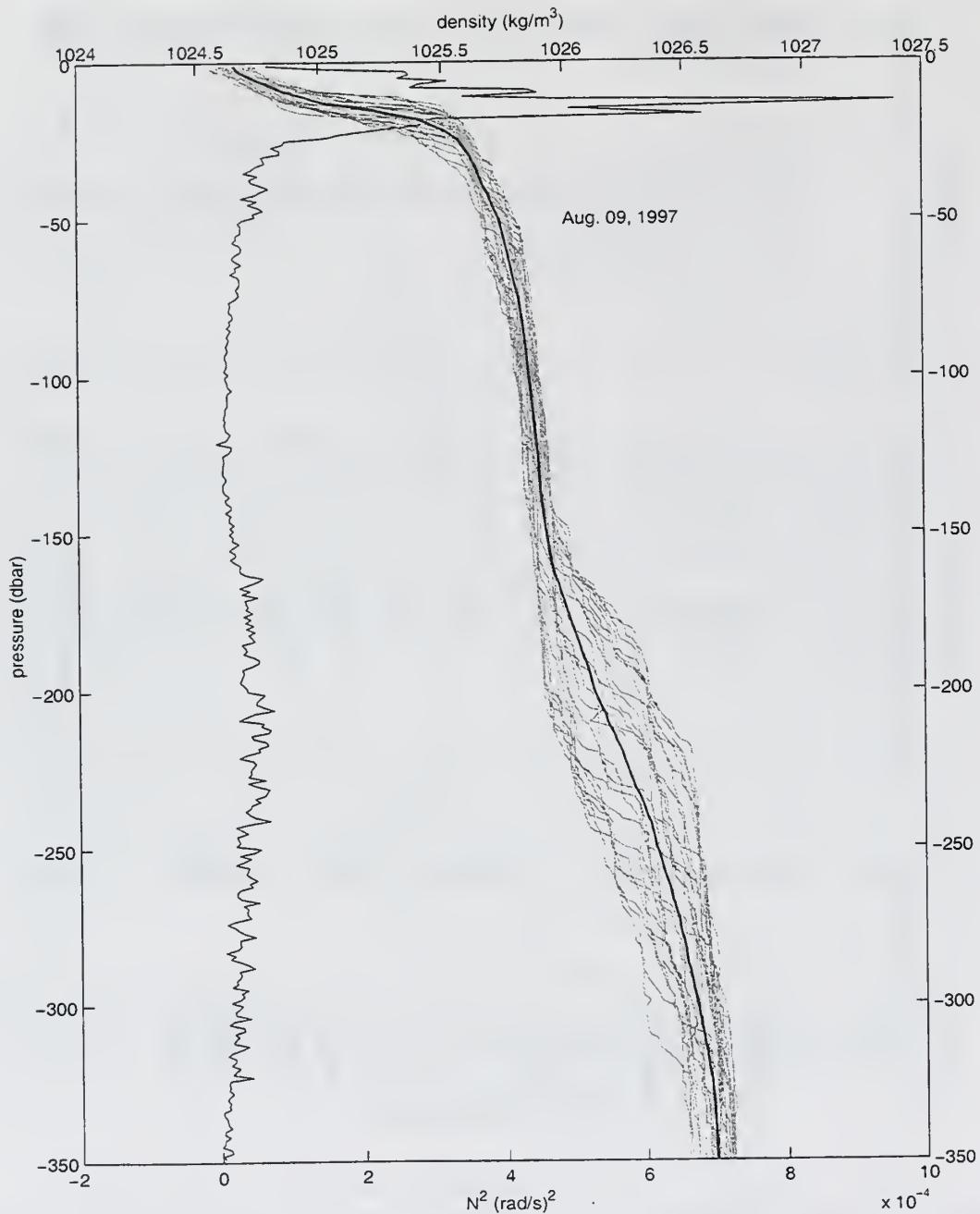
Figure 20. Density from Shallow station CTD casts (gray) with the average density (heavy black) and average $N^2(z)$ (left of density) for 09 August 1997.
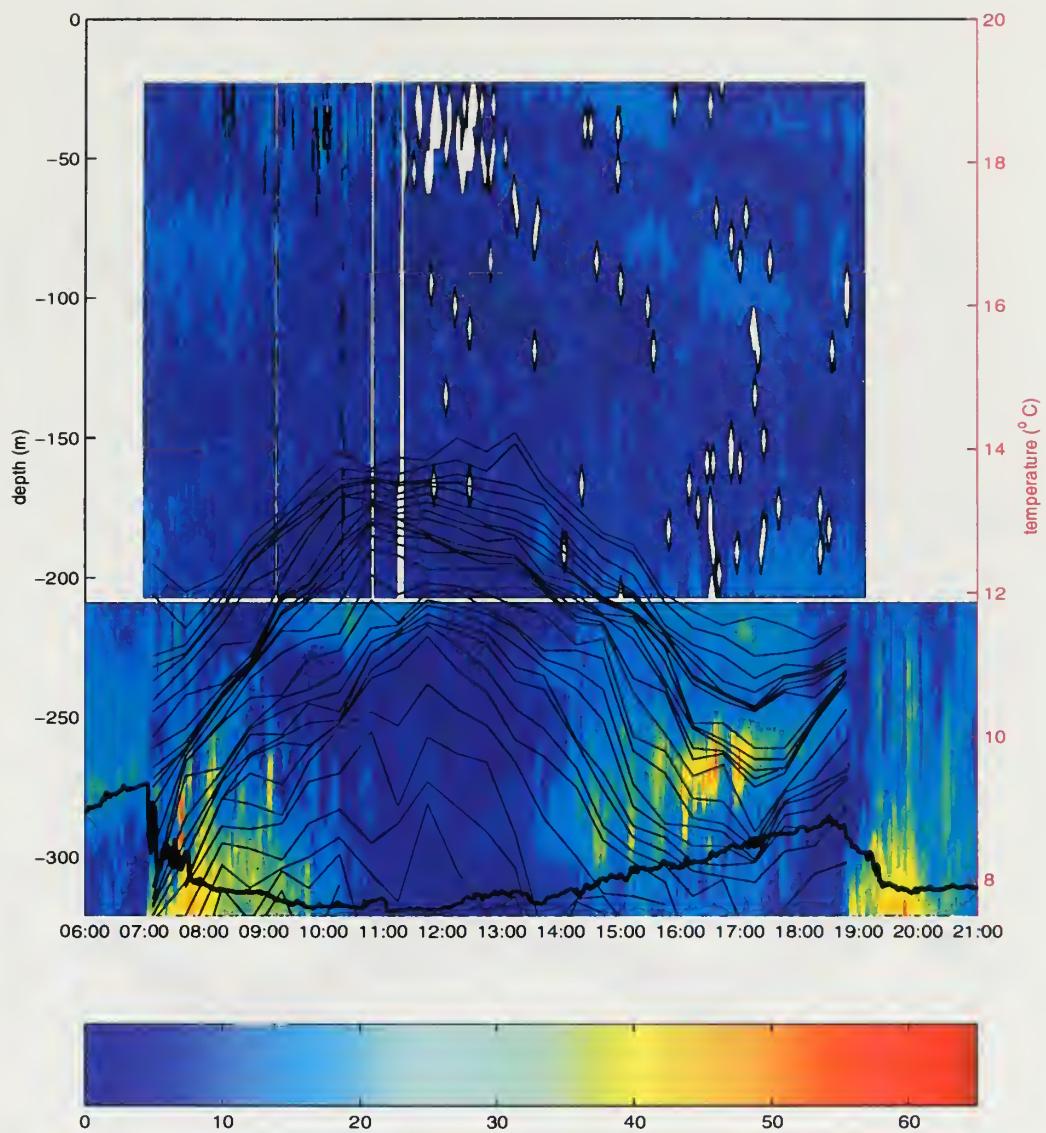
Figure 21. Speed contours (color, cm/s) from BB mooring and VM ADCP, 09 August 1997, showing the three events described in ch. IV with isopycnal contours (black lines, .025 kg/m^3 spacing, min 1026 / max 1026.675 kg/m^3) from CTD casts conducted at Shallow CTD station and temperature from the Alpha Omega thermistor (heavy black).

77
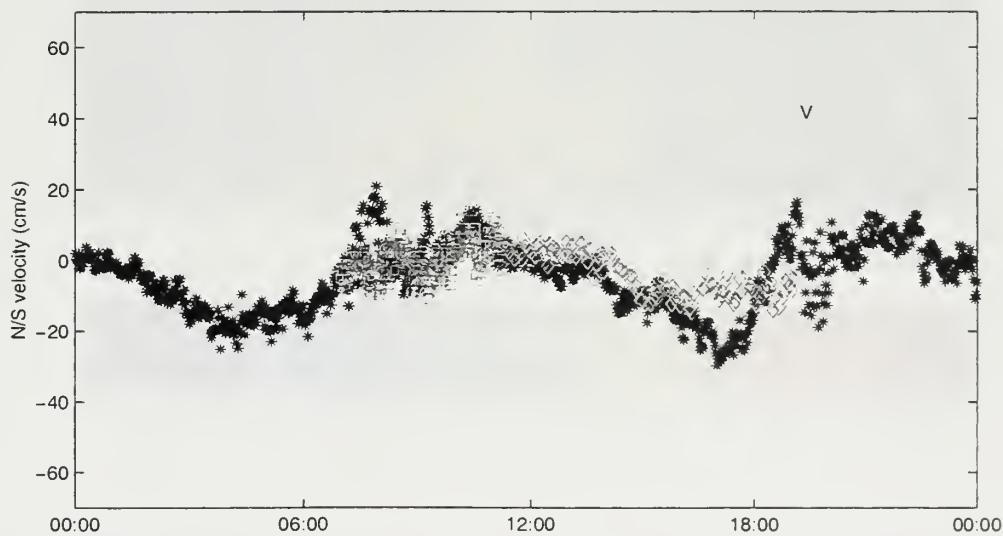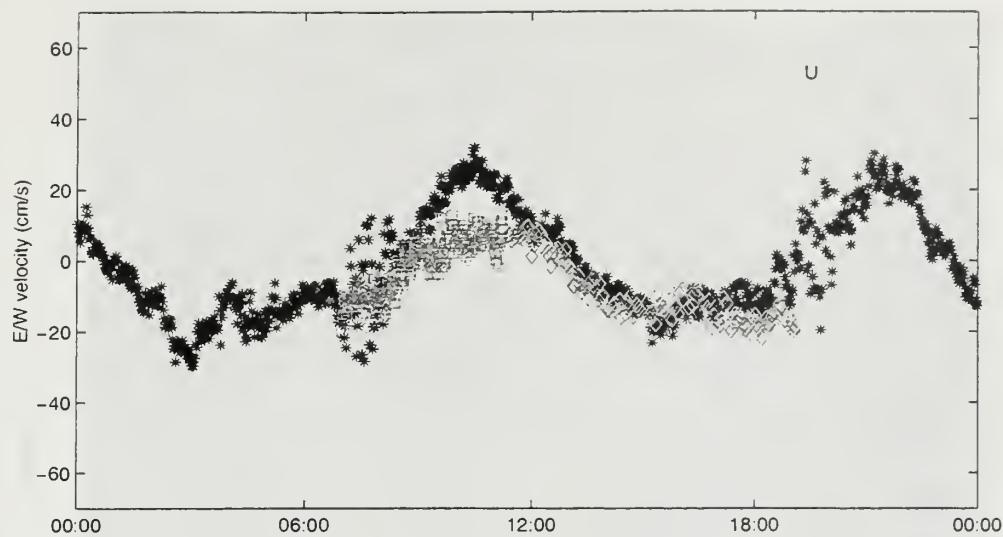
Figure 22. Comparison of VM-ADCP 1-min (squares) at 215 m, VM-ADCP 3-min (diamonds) at 215 m, and BB-ADCP (*) at 217 m. Upper(Lower) panel is E/W(N/S) component of velocity.
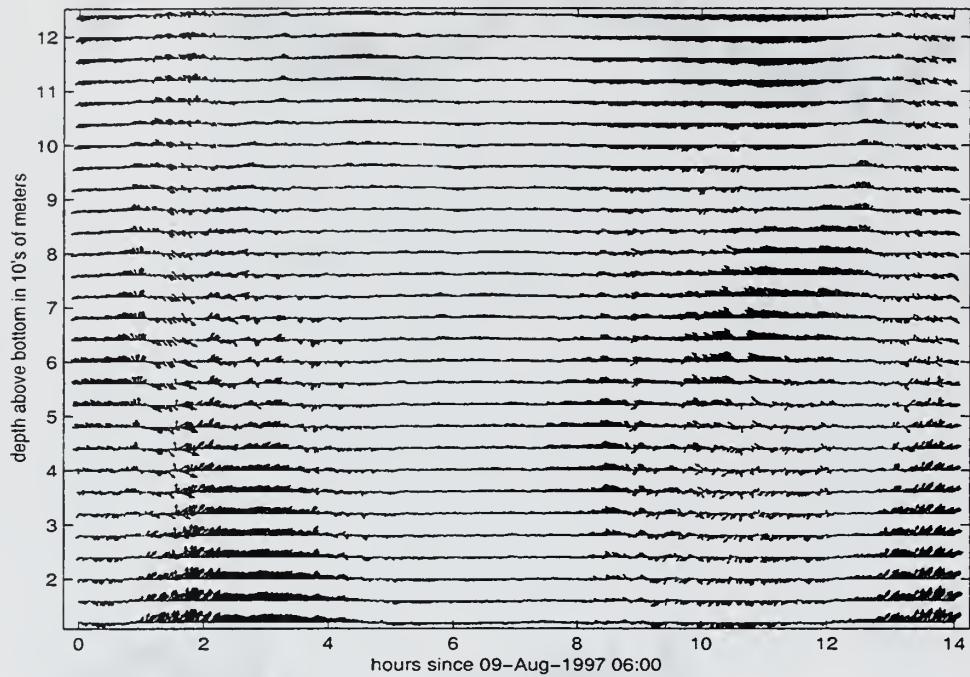
Figure 23. BB ADCP horizontal current speed (vector magnitude) and direction (true north up) for 09 August 1997. Maximum speed plotted is 69 cm/s.
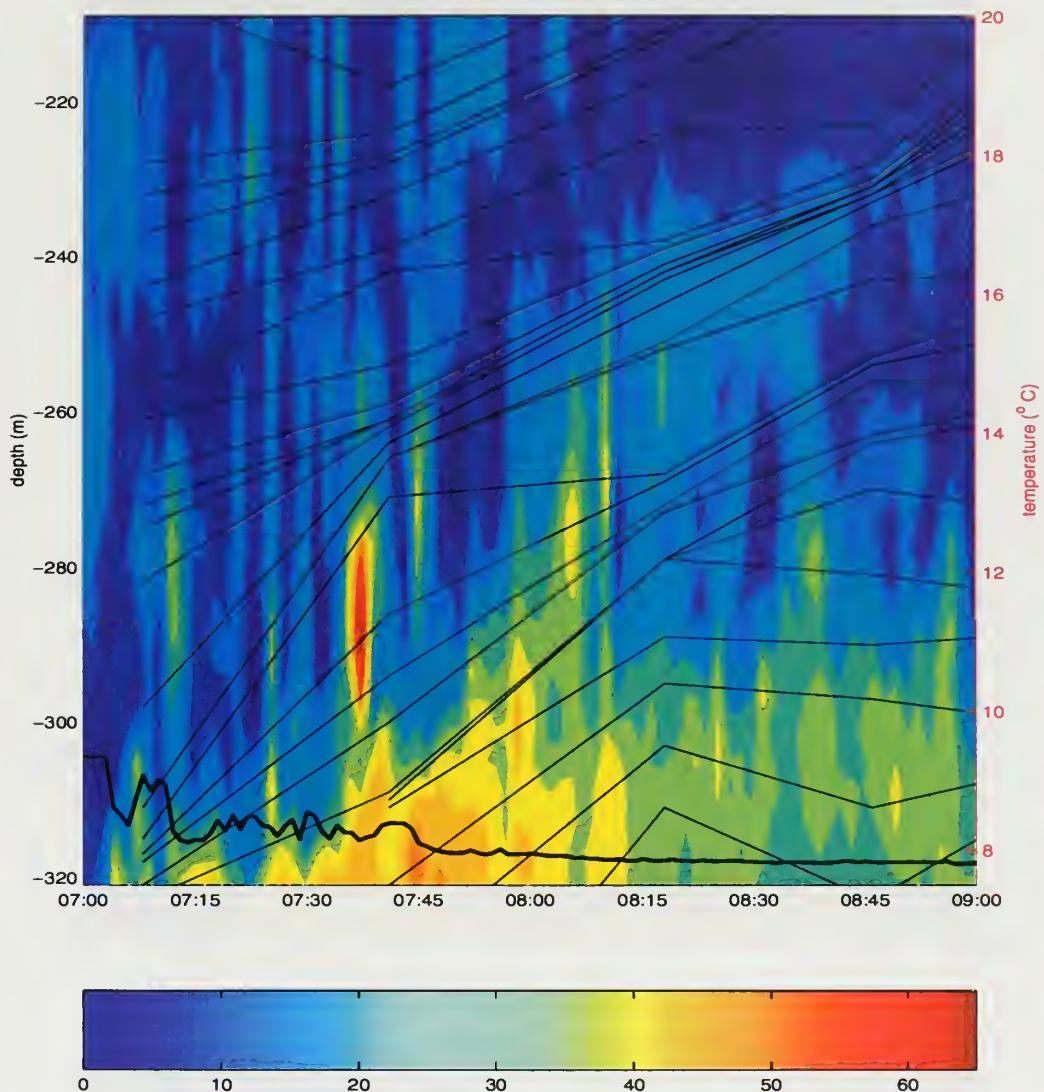
Figure 24. Speed contours (color, cm/s) from BB ADCP, 09 August 1997, showing the 0700 event with isopycnal contours (black, 0.025 kg/m³ spacing, min 1026.025 kg/m³ / max 1026.675 kg/m³) from CTD casts conducted at Shallow CTD station and temperature from the Alpha Omega thermistor (heavy black).
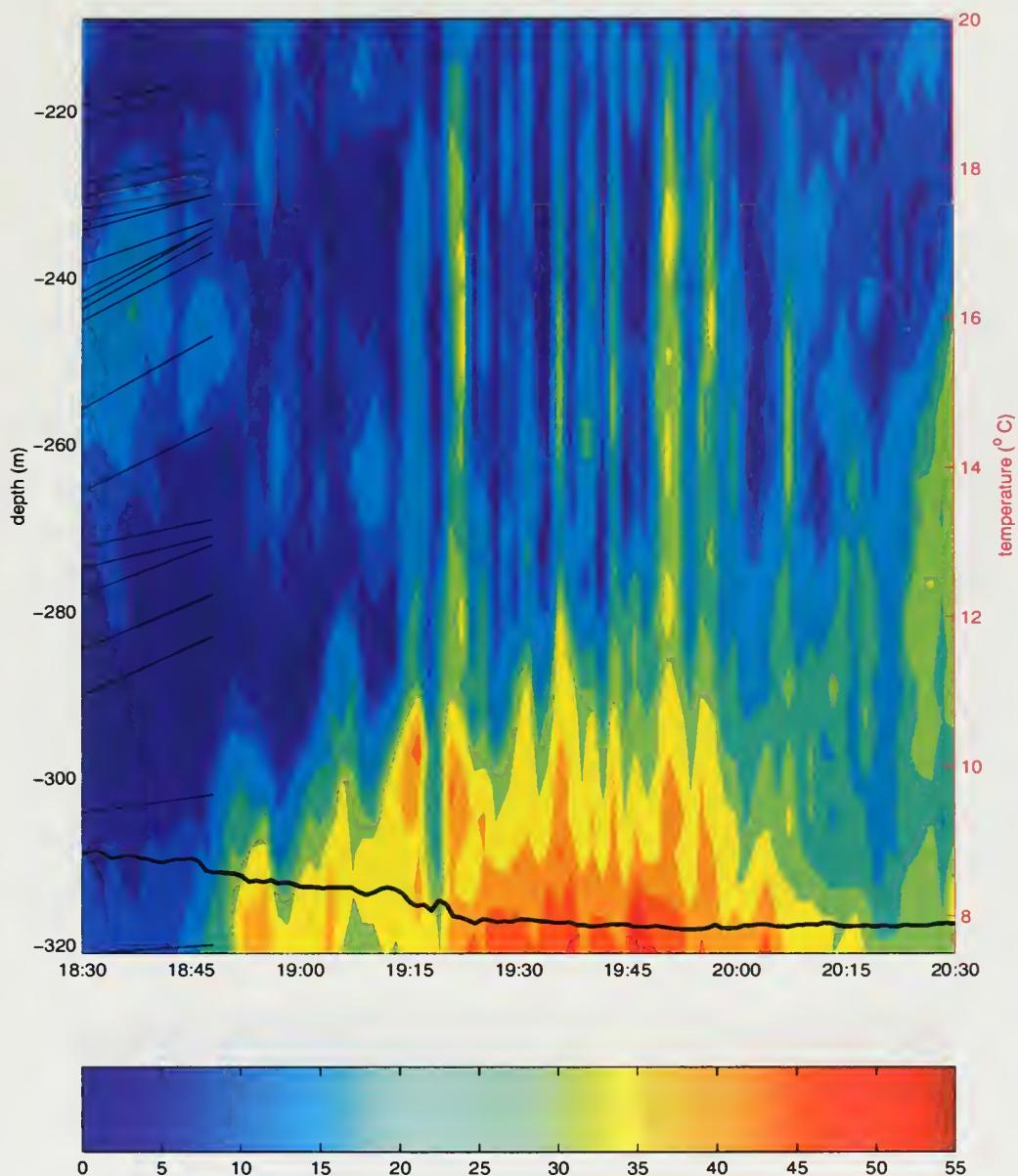
Figure 25. Same as Figure 24 showing the 1845 event on 09
August 1997 in detail. Minimum density plotted is 1026
kg/m³; maximum density plotted is 1026.475 kg/m³.
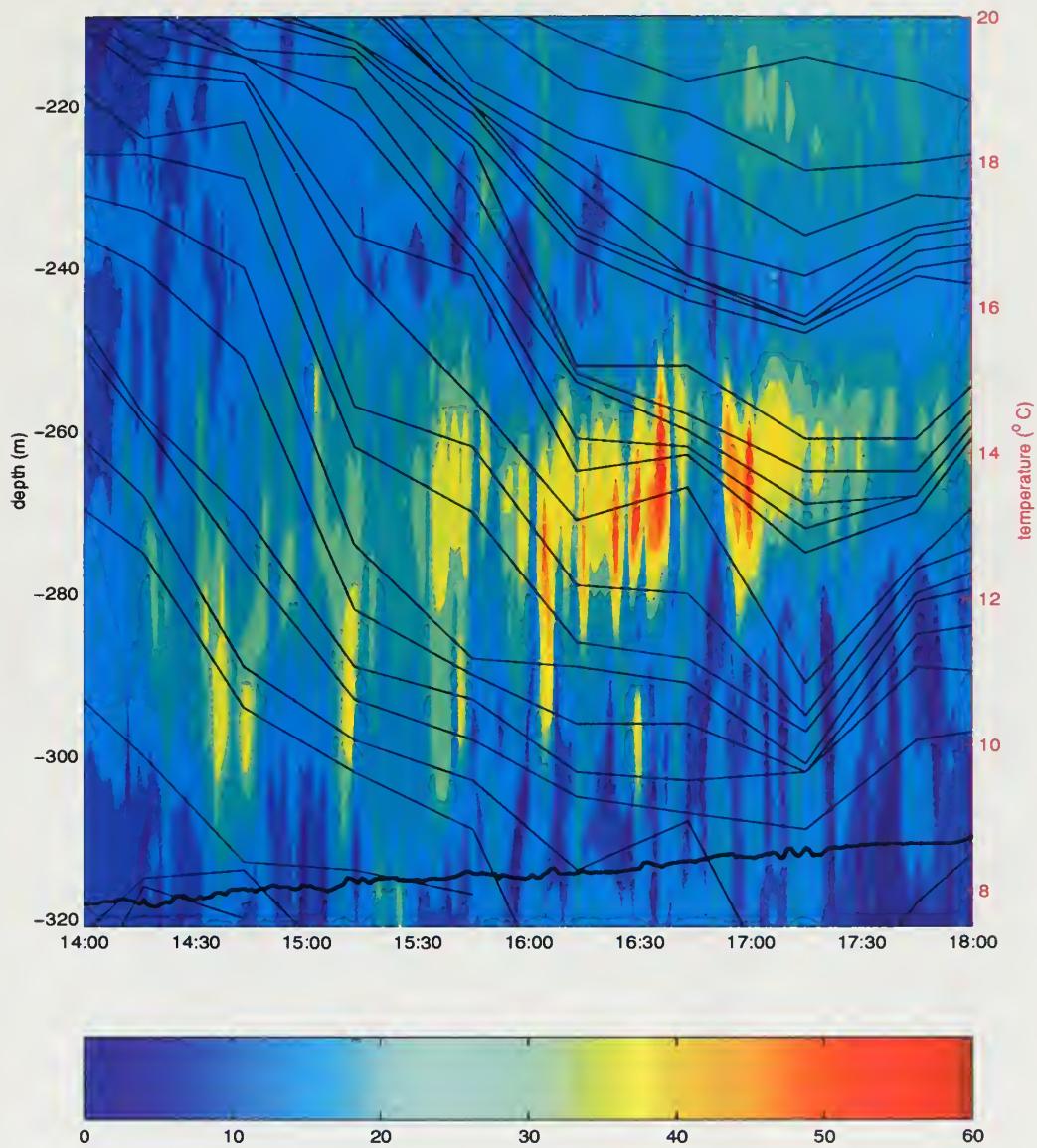
Figure 26.   Same as Figure 24 showing high frequency (2.5 min period) down-canyon current pulses on 09 August 1997 in detail.
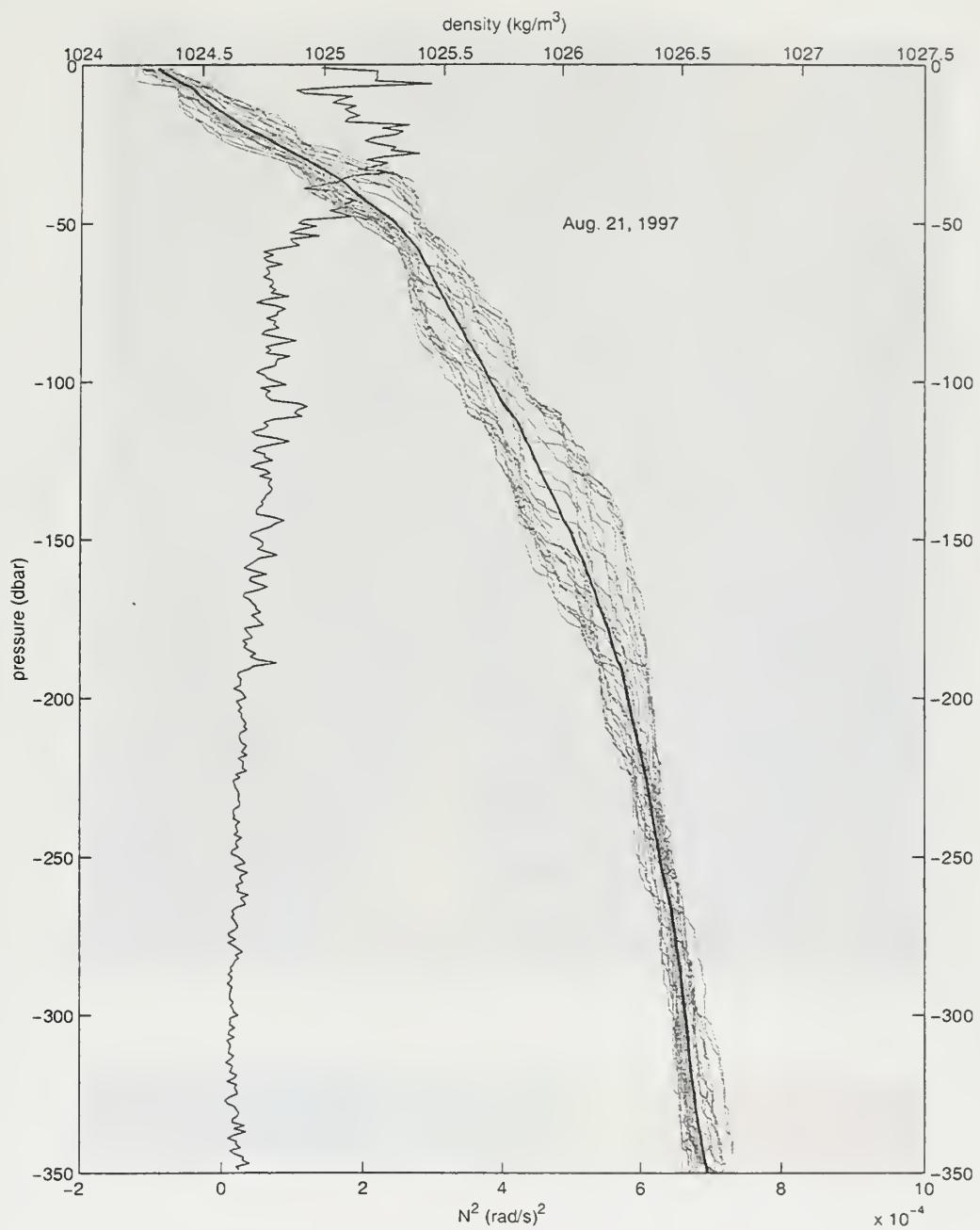
Figure 27. Density from Shallow station CTD casts (gray) with the average density (heavy black) and average $N^2(z)$ (left of density) for 21 August 1997.
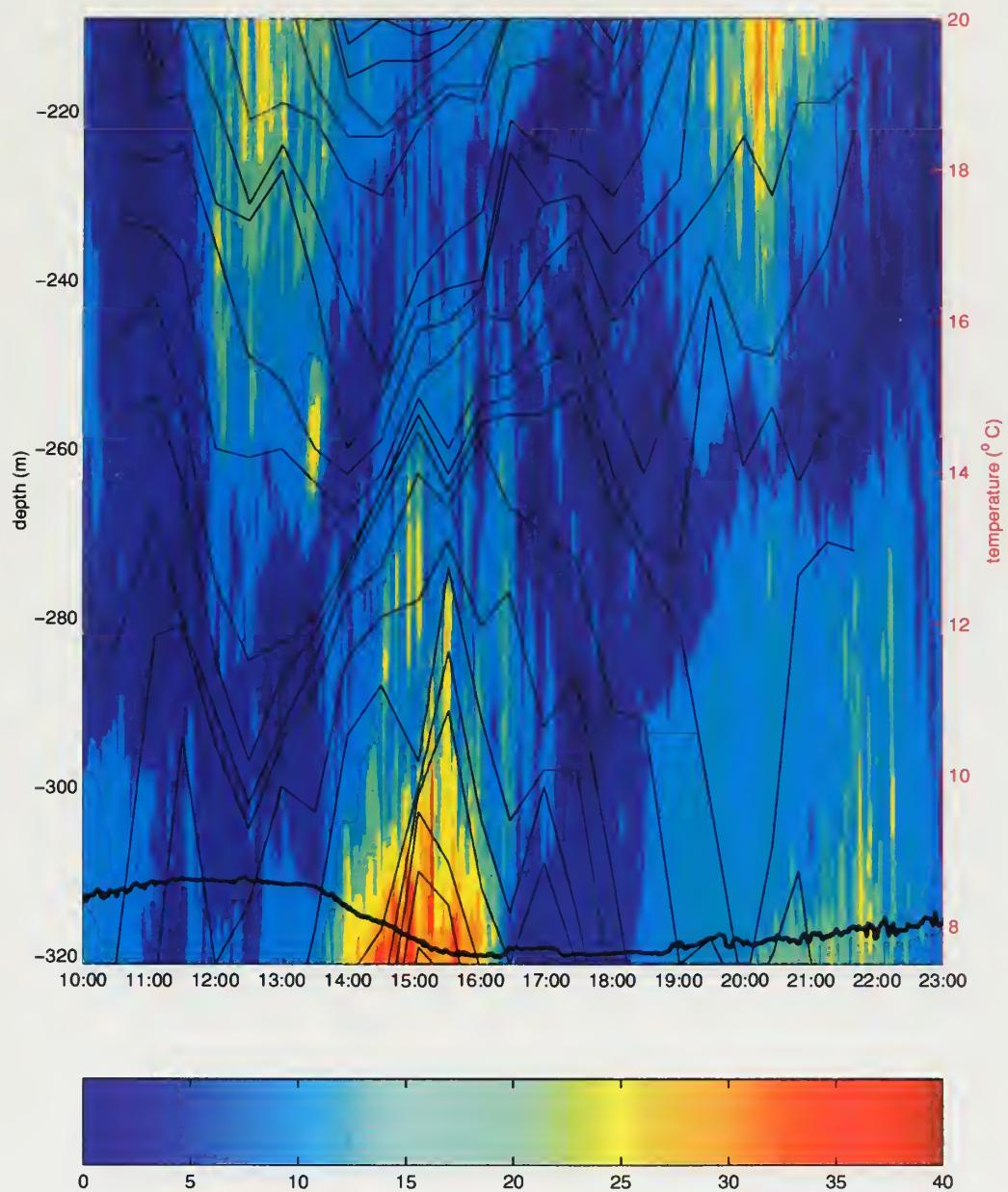
Figure 28. Same as Figure 24 showing 21 August 1997.
Maximum density is 1026.675 kg/m³; minimum density is
1026.200 kg/m³.
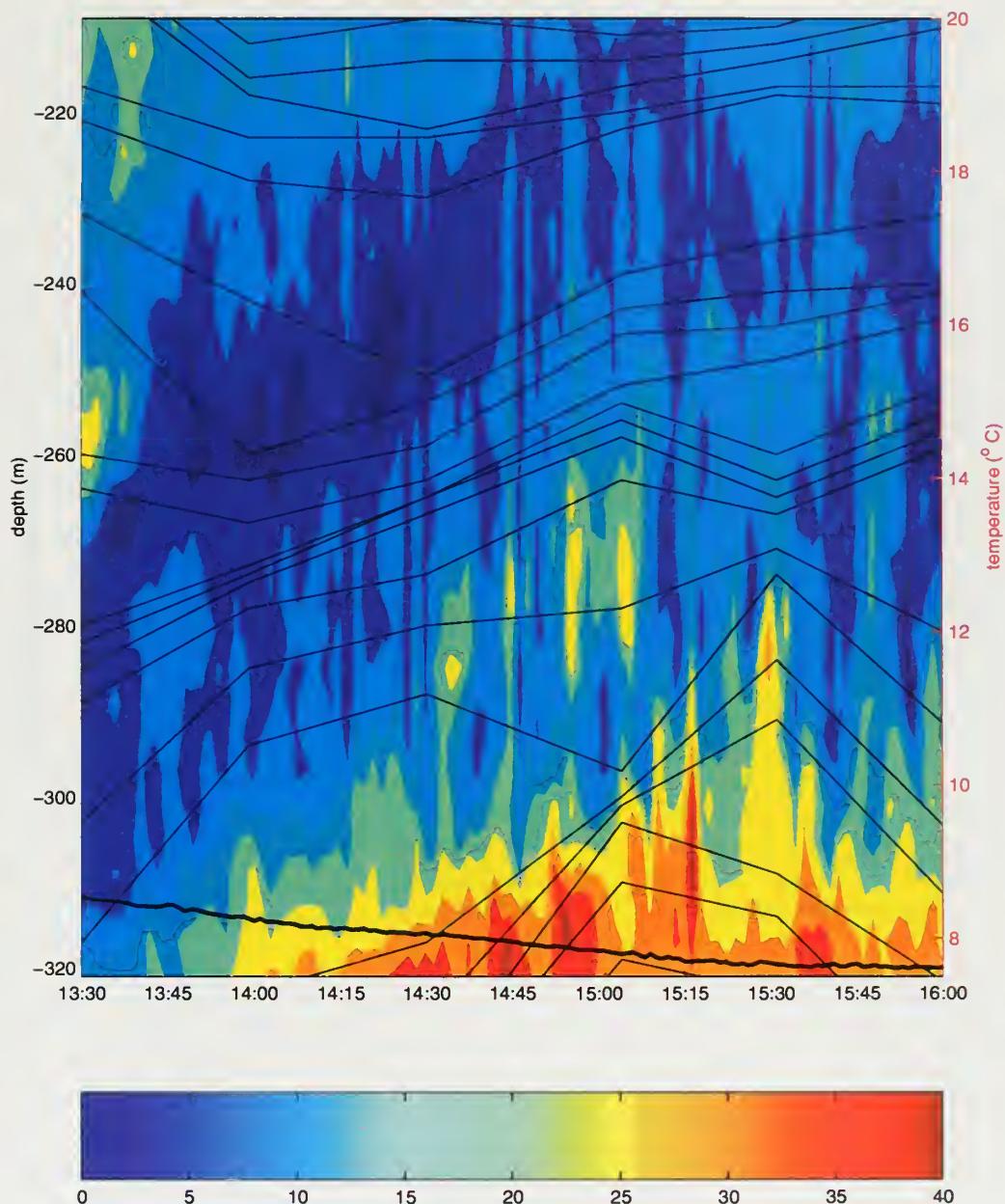
Figure 29. Same as Figure 28 showing close-up of event on 21 August 1997.
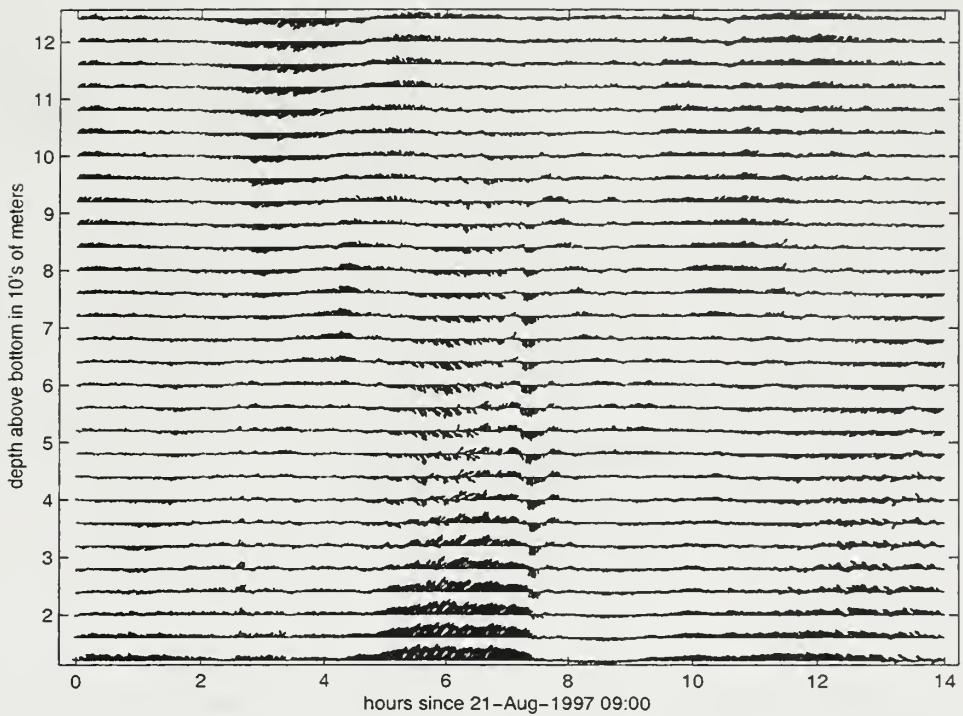
Figure 30. BB ADCP horizontal current speed (vector magnitude) and direction (true north up) for 21 August 1997. Maximum current plotted is 44 cm/s.
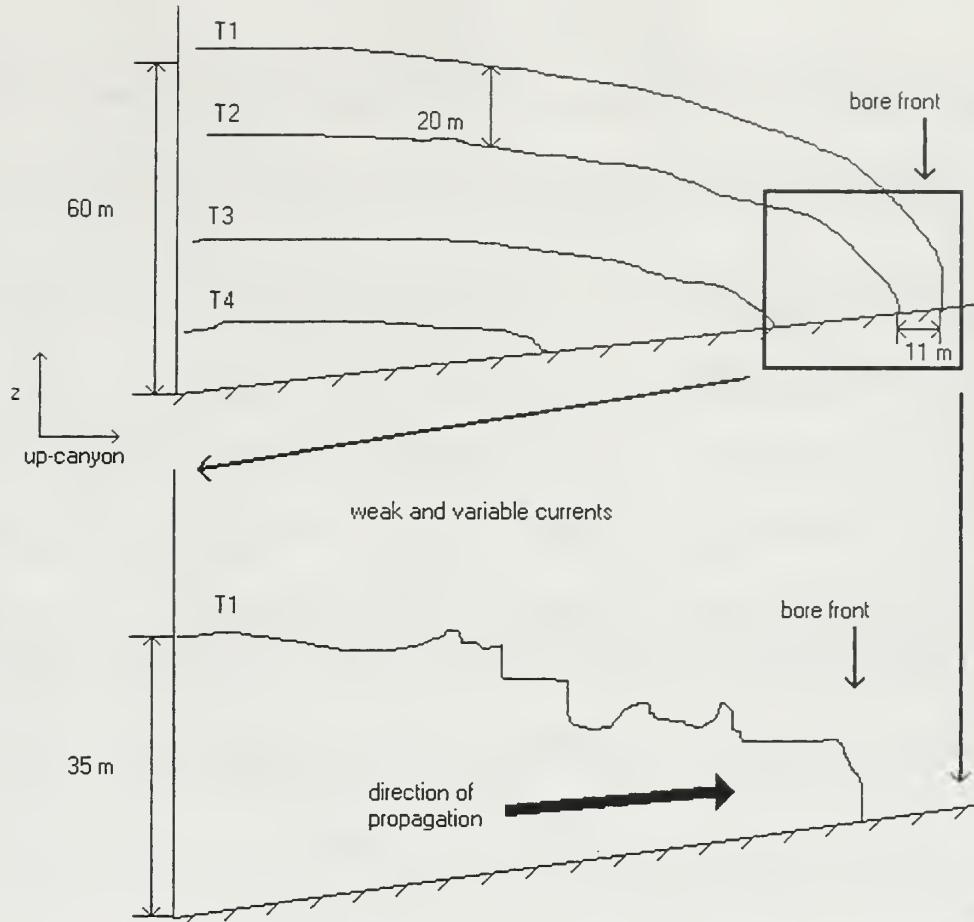
Figure 31. Conceptual image of the internal bore. T1 through T4 represent isotherms (0.25 °C apart) which terminate in a front in the up canyon direction. Lower frame is blow-up of T1 in the region of the bore showing turbulence-induced structure.
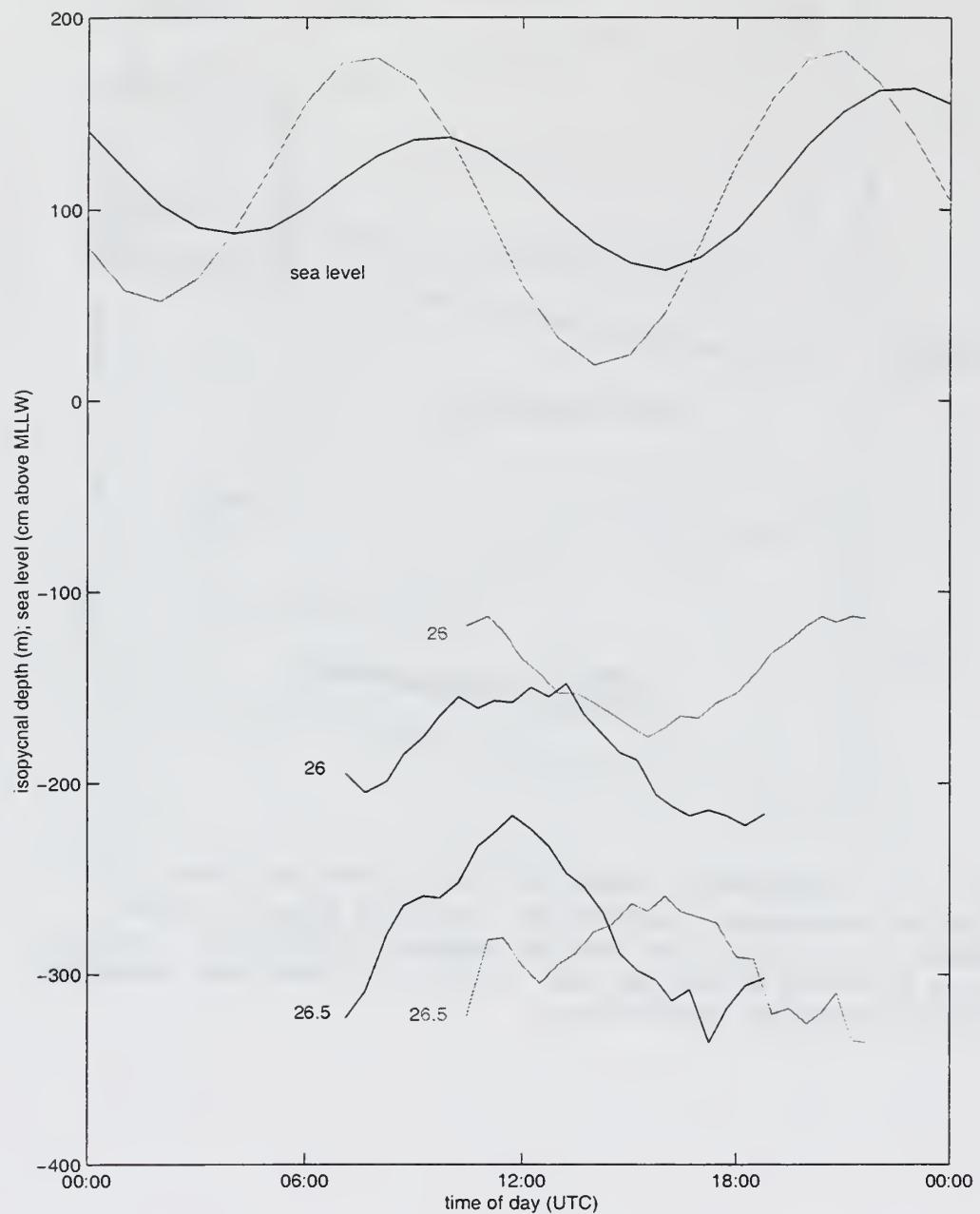
Figure 32. Sea level and isopycnal depths for 26 and 26.5 sigma t surfaces on 09 (black) and 21 August (gray).

LIST OF REFERENCES

Bogucki, D., T. Dickey, L.G. Redekopp, "Sediment resuspension and mixing by resonantly generated internal solitary waves", *J. Phys. Ocean.*, 27, pp. 1181-1196, 1997.

Cacchione, D.A., "Internal tides and sedimentation on continental slopes", Coastal Ocean Processes Symposium, Technical Report, pp. 49-52, 1999.

Caldwell, D.R., J.N. Moum, "Turbulence and mixing in the ocean", *Reviews of Geophys.*, Supplement, pp. 1385-1394, 1995.

Eriksen, C.C., "Internal wave reflection and mixing at Fieberling Guyot", *J. Geophys. Res.*, 103, C2, pp. 2977-2994, 1998.

Garrett, C.J.R, W.H. Munk, "Internal waves in the ocean", *Ann. Rev. Fluid Mech.*, 11, pp. 339-369, 1979.

Halpern, D., "Observations on short period internal waves in Massachusetts Bay", *J. Mar. Res.*, 29, 116, 1971.

Heard, J.A., *A Kinematic Model of Baroclinic Tidal Currents at the Head of the Monterey Submarine Canyon*, Master's Thesis, Moss Landing Marine Laboratories, San Jose State University, Moss Landing, California, 1992.

Holloway, P.E., "Internal hydraulic jumps and solitons at a shelf break region on the Australian north west shelf", *J. Geophys. Res.*, 92, C5, pp.5405-5416, 1987.

Holloway, P.E., E. Pelinovsky, T. Talipova, B. Barnes, "A nonlinear model of the internal tide transformation on the Australian north west shelf", *J. Phys. Ocean.*, 27, pp. 871-896, 1997.

Howell, T.L., W.S. Brown, "Nonlinear internal waves on the California continental shelf", *J. Geophys. Res.*, 90, C4, pp. 7256-7264, 1985.

Huthnance, J.M., "Internal tides and waves near the continental shelf edge", *Geophys. Astro. Fluid Dyn.*, 48, pp. 81-106, 1989.

Lafuente, J.G., T. Sarhan, M. Vargas, J.M. Vargas, "Tidal motions and tidally induced fluxes through La Linea submarine canyon, western Alboran Sea", *J. Geophys. Res.*, 104, C2, pp. 3109-3119, 1999.

Lee, C., R.C. Beardsley, "The generation of long nonlinear internal waves in a weakly stratified shear flow", *J. Geophys. Res.*, 3, pp. 453-462, 1974.

Kundu, P.K., *Fluid Mechanics*, Ch. 7, Academic Press, Inc., 1990.

Matsuyama, M., S. Ohta, T. Hibiya, H. Yamada, "Strong tidal currents observed near the bottom in the Suruga Trough, central Japan", *J. Ocean.*, 49, pp. 683-696, 1993.

Munk, W., "Internal waves and small scale processes", in *Evolution of Physical Oceanography*, edited by B.A. Warren and C. Wunsch, pp. 264-290, MIT Press, Cambridge, MA, 1981.

Munk, W., C. Wunsch, "The moon, of course...", *Oceanography*, 10, pp. 132-134, 1997.

Ostrovsky, L.A., Y.A. Stepanyants, "Do internal solitons exist in the ocean?", *Reviews of Geophys.*, 27, pp. 293-310, 1989.

Petruncio, E.T., *Observations and Modeling of the Internal Tide in a Submarine Canyon*, PhD Dissertation Naval Postgraduate School, Monterey, California, 1996.

Petruncio, E.T., L.K. Rosenfeld, J.D. Paduan, "Observations of the internal tide in Monterey Canyon", *J. Phys. Ocean.*, 28, pp. 1873-1903, 1998.

Pugh, D.T., *Tides, Surges and Mean Sea-Level*, pp. 347-359, John Wiley and Sons LTD., 1987.

Ramp, S.R., L.K. Rosenfeld, T.D. Tisch, M.R. Hicks, "Moored observations of the current and temperature structure over the continental slope off central California", *J. Geophys. Res.*, 102, C10, pp. 22,877-22,902, 1997.

Rosenfeld, L.K., "Baroclinic semidiurnal tidal currents over the continental shelf off northern California", *J. Geophys. Res.*, 95, C12, pp. 22,153-22,172, 1990.

Rosenfeld, L.K., J.D. Paduan, E.T. Petruncio, J.E. Goncalves, "Numerical simulations and observations of the internal tide in a submarine canyon", *'Aha Huliko'a Proceedings*, Hawaiian Winter Workshop, 1999.

Shea, R.E., W.W. Broenkow, "The role of internal tides in the nutrient enrichment of Monterey Bay, California", *Estuarine, Coastal and Shelf Science*, 15, pp. 57-66, 1982.

Shepard, F.P., N.F. Marshall, P.A. McLoughin, and G.G. Sullivan, "Currents in submarine canyons and other sea valleys", *AAPG Studies in Geology No. 8*, American Assoc. of Petroleum Geologists, 1979.

Slinn, D.N., J.J. Riley, "Turbuent mixing in the oceanic boundary layer caused by internal wave reflection from sloping terrain", *Dyn. Atmos. And Oceans*, 24, pp. 51-62, 1996.

Stanton, T.P., L.A. Ostrovsky, "Obeservations of highly nonlinear internal solitons over the continental shelf", *Geophys. Res. Letters*, 25, 11, pp. 2695-2698, 1998.

Takeuchi, K., T. Hibiya, "Numerical simulation of baroclinic tidal currents in Suruga Bay and Uchiura Bay using a high resolution level model", *J. Ocean*, 53, pp.539-552, 1997.

Thorpe, S.A., "Thermal fronts caused by internal gravity waves reflecting from a slope", *J. Phys. Ocean.*, 22, pp. 105-108, 1992.

Werner, F.E., "Tidal hydrodynamics, quantitative aspects", *Encyclopedia of Earth System Science*, 4, pp. 351-367, 1992.

INITIAL DISTRIBUTION LIST

1. Defense Technical Information Center 2
    8725 John J. Kingman Road, Ste 0944
    Ft. Belvoir, Virginia 22060-6218

2. Dudley Knox Library 2
    Naval Postgraduate School
    411 Dyer Rd.
    Monterey, California 93943-5101

3. Dr. Leslie K. Rosenfeld 2
    Department of Oceanography, Code OC/Ro
    833 Dyer Rd., Rm 328
    Monterey, California 93943-5002

4. Dr. Timothy Stanton 1
    Department of Oceanography, Code OC/St
    833 Dyer Rd., Rm 328
    Monterey, California 93943-5002

5. LT Scott Key 1
    593 B Michelson Rd.
    Monterey, California 93940

6. Dr. Eric Kunze 1
    Applied Physics Lab, University of Washington
    1013 NE 40th
    Seattle, Washington 98105-6698

7. Dr. Steve Meacham 1
    Division of Ocean Sciences, Rm 725
    National Science Foundation
    Arlington, Virginia 22230

8. Dr. Lou Goodman 1
    Office of Naval Research, 322 PO
    800 N. Quincy St.
    Arlington, Virginia 22230

9. Chairman, Code OC/Gd 1
    Department of Oceanography
    833 Dyer Rd., Rm 328
    Monterey, California 93943-5002

10. Dr. Jim Bellingham, MBARI 1
    PO Box 628
    Moss Landing, California 95039-0628

11. Dr. Eric Isweire 1
    Division of Ocean Sciences, Rm 725
    National Science Foundation
    Arlington, Virginia 22230

12. Mr. James Key 1
    11010 NE 68th, #606
    Kirkland, Washington 98033